Highly potent novel multi-armoured IL13Rα2 CAR-T subverts the immunosuppressive microenvironment of Glioblastoma

Maurizio Mangolini[1], Saket Srivastava[1], Emily Souster[1], Yajing Yang[1], Huimin Wang[1], Rajesh Karattil[1], Liam Schultz[1], Biao Ma[1], Diana Pombal[1], Matthew Greenig[2], Aubin Ramon[2], Pietro Sormanni[2], Shaun Cordoba[1], Shimobi Onuoha[1]

[1]Chimeris UK, The Works, Unity Campus, London Road, Cambridge, CB22 3EE

[2]Centre for Misfolding Diseases, Yusuf Hamied Department of Chemistry, University of Cambridge, Lensfield road, CB2 1EW Cambridge, UK

ABSTRACT

Glioblastoma (GBM) remains one of the most challenging and lethal brain cancers, with limited treatment options. While CAR-T cells have shown promise in some patients, sustaining T-cell activity and overcoming the immunosuppressive tumour microenvironment (TME) remain significant hurdles. Here, we present an armoured CAR-T cell design to address these challenges and enhance persistence in GBM tumours. We developed a highly specific humanised single-domain antibody (VHH) targeting IL13Rα2 and included it alongside four additional modular elements in a single retroviral vector for CAR-T generation. Our results demonstrate that this single-cassette CAR-T cell design possesses high resilience against TGF-β-mediated immunosuppression, enhanced tumour-killing capacity through IL-12 secretion while maintaining a favourable safety profile, extended persistence in the host, and an additional layer of safety control through the incorporation of a suicide switch. Importantly, despite its complexity, the construct can still be manufactured efficiently. These advancements represent a significant step forward in addressing key challenges associated with CAR-T cell therapy in solid tumours.

INTRODUCTION

Glioblastoma (GBM) is one of the most aggressive and lethal forms of brain cancer, with a dismal prognosis despite current standard treatments and the implementation of multimodal treatment strategies. Unfortunately, at present day, the prognosis for glioblastoma remains poor with a median survival of less than 15 months from initial diagnosis, a 2-year survival rate of approximately 26-33% and a 5-year survival rate estimated at just 6.8%[1,2].

In recent years, chimeric antigen receptor (CAR) T cell therapy has emerged as a promising immunotherapeutic approach for treating GBM[3]. Among the various targets explored, interleukin-13 receptor alpha 2 (IL13Rα2) has garnered significant attention as a potential CAR-T cell target for this disease indication. IL13Rα2 is a monomeric high-affinity receptor for interleukin-13 (IL-13) that is overexpressed in most GBM tumours, with studies reporting its presence in 60-75% of cases. Importantly, IL13Rα2 expression is minimal in normal brain tissue, making it an attractive tumour-specific target[4,5,6]. The receptor's overexpression is associated with the mesenchymal GBM subtype and correlates with poor patient survival, further underscoring its relevance as a therapeutic target[7].

CAR-T cells engineered to target IL13Rα2 have shown promising results in preclinical studies triggering a potent anti-tumour immune response. Furthermore, recent clinical trials evaluating IL13Rα2-targeted CAR-T cells in GBM patients have shown encouraging results, with evidence of tumour regression and improved survival in some cases[8,9,10,11]. However, challenges such as antigen loss and limited T-cell persistence have been observed. One way to overcome the challenges faced by CAR-T cell therapy in treating solid tumours like GBM is to develop "armoured" CAR-T cells with enhanced capabilities.

Similarly to most solid tumours, GBM employs various immune-evasive strategies within their tumour microenvironment (TME) that result in treatment resistance. These mechanisms pose substantial challenges for CAR-T cells, hindering their ability to mount effective antitumor responses and achieve the robust expansion necessary for significant tumour reduction. Among these, the Transforming Growth Factor beta (TGF-β1/TGF-βR2) signalling pathway is particularly significant in promoting T cell dysfunction and limiting their proliferation[12,13,14]. Enhancing CAR-T cells with the ability to produce anti-tumour cytokines is also a promising strategy to overcome the challenges posed by the hostile TME. Interleukin-12 (IL-12) stands out among these cytokines for its remarkable anti-tumour capacity. However, the clinical application of IL-12 has faced significant hurdles due to its potent systemic toxicity[15,16]. Indeed, multiple experimental models and clinical trials have revealed toxicity profiles associated with systemic IL-12 exposure, which has hampered its progression in therapeutic development[17].

Here we show a novel armoured CAR-T cell targeting IL13Rα2, which addresses several key challenges associated with CAR-T cell treatment of GBM. Our approach combines a newly developed, highly specific, humanized single-domain antibody (VHH) against IL13Rα2 with a fourth-generation CAR design that incorporates multiple functional enhancements within a single retroviral vector. This advanced CAR construct includes: -a TGF-β receptor-blocking antibody; - a constitutively active form of the GM-CSF intracellular receptor region; -an engineered single-chain IL-12 sequence; - a modified version of HER2 as a suicide switch for controlled cell elimination. We demonstrate that primary T cells expressing this construct show superior performance compared to conventional CAR-T cells, exhibiting enhanced tumour cell killing, improved proliferation, and prolonged persistence. The blockade of TGF-β signalling significantly enhances the engineered T cells' resistance to immunosuppression, while the attenuated IL-12 activates bystander NK and T cells without observable toxicity. Furthermore, the incorporation of a suicide gene, activated by the FDA-approved drug Trastuzumab

71 emtansine (T-DM1), provides a crucial safety mechanism for the controlled elimination of the
72 engineered cells. *In vitro* and *in vivo* data confirmed the efficacy, survival, and safety profile of
73 these armoured CAR-T cells, even at low doses. Notably, despite the complexity of the
74 construct, we demonstrate manufacturing feasibility in a Good Manufacturing Practices (GMP)
75 - compliant setting. Altogether, our findings offer a promising new avenue for the treatment of
76 GBM and potentially other IL13Rα2-expressing malignancies representing a significant step
77 forward in the field of CAR-T cell therapy for solid tumours.

78 **RESULTS**

79 ***In vitro* screening identifies lead IL13Rα2 VHH for CAR-T cells**

80 The targeting domain of CARs is their most critical component for recognizing and interacting
81 with the desired target antigen. To develop a new CAR targeting IL13Rα2, we created a specific
82 nanobody, due to their advantages in terms of low immunogenicity and small size[18]. The
83 discovery of the IL13Rα2-specific nanobody was achieved through a combination of
84 immunization, phage display, and deep repertoire mining, followed by humanization and
85 functional screening (Figure 1a). In brief, after immunizing alpacas, we generated a phage
86 display library enriched against IL13Rα2, using IL13Rα1 as a deselection target to ensure high
87 specificity for IL13Rα2 while avoiding cross-reactivity with IL13Rα1.

88 Next-generation sequencing (NGS) was then performed on the enriched library, and cluster
89 analysis identified potential binders. The analysis focused on extracting complementarity-
90 determining regions (CDRs) 1, 2, and 3, which were computationally combined to generate
91 artificial sequences for similarity clustering, with the idea that VHHs with similar CDRs should
92 bind the same epitope. Homology groups were formed using a distance matrix that prioritized
93 chemical differences and similarities between amino acids, rather than simpler sequence-
94 identity (Supplementary Figure 1a). The highest frequency sequence from each group was

selected for further characterisation. This approach effectively sampled the diversity of the screened library and reduced the risk of clonal dominance.

Parallel to NGS analysis, traditional panning and clone selection by colony picking were also performed, yielding complementary insights. Parallel to NGS analysis, traditional panning and clone selection by colony picking were also performed, yielding complementary insights. A total of 50 clusters were initially identified, with 20 clusters progressing to production and subsequent functional evaluation (Figure 1b,c). Binding specificity assays identified eight molecules that bound IL13Rα2 without cross-reactivity to IL13Rα1. However, despite the extensive diversity of the library, repeated rounds of panning narrowed the functional binders to two primary sequences. This observation suggests a potential bias in phage display selection that was not mirrored in the broader diversity identified through NGS.

Half maximal effective concentration (EC_{50}) and thermal stability (T_m) analysis revealed that the majority of the selected binders exhibited favourable melting temperatures, indicative of robust biophysical properties in addition to specific binding (Figures 1d,e). Based on these combined biophysical and functional analyses, clone C1.1 from cluster 1 emerged as the lead candidate for incorporation into the IL13Rα2 CAR, designated IL13Rα2 c1.1.

We then performed humanisation of the Clone c1.1 using the AbNatiV VHH humanisation pipeline, reported in Ramon et al. [19]. This AI-based approach samples humanising mutations ensuring retention of binding affinity and favourable VHH biophysical properties (Figure 1f). The humanized variants $c1.1^{en}$ and $c1.1^{ex}$, respectively from the enhanced and exhaustive AbNatiV humanisation pipelines[19] showed equivalent stability and specificity compared to the wild-type counterpart. To further assess the specificity of these VHHs for IL13Rα2 and minimize the risk of off-target binding effects, we conducted an extensive cross-reactivity study. This study evaluated the binding of the VHHs against approximately 6,000 native human membrane proteins. Remarkably, all three clones demonstrated minimal cross-reactivity with

120 other proteins. Among them, c1.1^{en} exhibited the strongest specific binding to IL13Rα2
121 (Supplementary Figure 1b).
122 Clones c1.1, c1.1^{en} and c1.1^{ex} were then inserted in a retroviral vector encoding a CAR
123 construct with CD28 and CD3ζ intracellular signalling domains (Figure 1g). Functional assays
124 demonstrated robust killing of IL13Rα2-positive target cells across all tested CAR variants
125 (Figure 1h and Supplementary Figure 1c,d). Notably, the humanized variant c1.1^{en} exhibited
126 lower levels of background activity or "tonic signalling" compared to both the wild-type llama-
127 derived CAR and the exhaustive-humanized c1.1^{ex} CAR (Figure 1i and Supplementary Figure
128 1e). This reduction in background activity is likely due to improved biophysical properties,
129 such as increased solubility and thermal stability, engineered during the humanization process.
130 Further validation was conducted using CellTrace Violet (CTV) proliferation assays on
131 IL13Rα2-positive and IL13Rα2-negative SupT1 cells. IL13Rα2 C1.1^{en} CAR exhibited
132 minimal off-target activity against IL13Rα1, corroborating its specificity and reduced
133 background signalling (Figure 1j). These results highlight the advantages of the engineered
134 humanized clone C1.1^{en}, demonstrating its suitability for clinical development and its potential
135 to mitigate adverse effects associated with CAR tonic signalling.

136 **dsFvTBRII/CCR overcomes the inhibitory effects of TGF-β and induces CAR-T cell**
137 **persistence**

138 TME-induced T cell inhibition and reduced persistence are among the major factors limiting
139 the efficacy of CAR-T cells in solid tumours[20]. To overcome these limitations, we designed a
140 fusion protein containing two key elements: an extracellular region consisting of a blocking
141 antibody for the TGF-β receptor II (TBRII) and the transmembrane and truncated intracellular
142 domains of the granulocyte-macrophage colony-stimulating factor (GM-CSF) receptor as a
143 chimeric costimulatory receptor (CCR) (Figure 2a). This innovative architecture leverages the
144 disulfide bond of the TBRII antibody region to achieve constitutive downstream activity of the

145 receptor. We first validated the blocking functionality of the disulfide-stabilized single-chain
146 variable fragment (dsFv) antibody derived from the original Fab sequence. Using a reporter
147 cell line that quantifies TGF-β response through secreted embryonic alkaline phosphatase
148 (SEAP) production, we demonstrated that the dsFv antibody retained the TGF-β blocking
149 capacity of the original Fab version (Figure 2b). Subsequently, we evaluated the function of
150 the intracellular component. We generated two single cassette constructs expressing the
151 dsFvTBRII region fused with different orientations of the GM-CSF receptor chains: alpha-beta
152 and beta-alpha. The overexpression of these constructs in Jurkat cells revealed that the beta-
153 alpha orientation was more potent in activating STAT5 (Figure 2c). This finding was further
154 corroborated using GM-CSF reporter cell lines (Supplementary Figure 2a). Moreover, we
155 confirmed that the final chimeric receptor design (dsFvTBRII/CCR) maintained its TGF-β
156 blocking functionality when tested using TGF-β reporter cells (Figure 2d). To assess whether
157 the dsFvTBRII/CCR module would enhance CAR-T cell resistance to TGF-β and improve their
158 persistence, we integrated this construct into the IL13Rα2 c1.1^{en} CAR design, separating the
159 two components with a T2A ribosomal skipping site. Comparative analysis revealed that CAR-
160 T cells incorporating the dsFvTBRII/CCR module exhibited reduced susceptibility to TGF-β
161 pathway activation, measured by decreased SMAD2/3 phosphorylation (Figure 2e).
162 Furthermore, in cytokine-deprived *in vitro* culture conditions (Figure 2f), control cells incurred
163 complete cell death within 10 days, whereas cells overexpressing the CCR maintained viability
164 for up to 40 days, similar to what has been previously shown using a GM-CSF based CCR[21]
165 (Figure 2g). To determine whether the extended viability observed in CAR-T cells expressing
166 the CCR module was accompanied by enhanced proliferative capacity, we conducted a dye
167 dilution assay to track cell division over 7 days. Our results demonstrated that CAR-T cells
168 incorporating the CCR module underwent multiple rounds of proliferation, significantly
169 outperforming the control cells (Figure 2h). This finding was further corroborated by the rapid

170 increase in the proportion of CCR-expressing CAR-T cells within the total cell population over
171 time (Figure 2i). To further validate the efficacy of our dsFvTBRII/CCR module, we employed
172 the well-characterized CD19 CAR-T cell model as an additional experimental system. *In vitro*
173 experiments demonstrated that overexpression of the dsFvTBRII/CCR construct in CD19
174 CAR-T cells conferred partial protection against the cytotoxic inhibitory effects of TGF-β
175 (Supplementary Figure 2b). Moreover, we observed that cells incorporating this additional
176 module displayed extended longevity compared to those expressing only the CAR construct,
177 suggesting that the ability of the dsFvTBRII/CCR to enhance CAR-T cells' persistence is
178 independent of the upstream CAR architecture (Supplementary Figure 2c,d). Collectively,
179 these results indicate that the incorporation of the dsFvTBRII/CCR module confers enhanced
180 resistance to TGF-β-mediated immunosuppression and significantly extends the survival and
181 the proliferative potential of CAR-T cells in the absence of exogenous cytokine support,
182 potentially overcoming some of the challenges of the tumour microenvironment.

183 **Development of a scIL12 with an improved safety profile**

184 IL-12 is a potent pro-inflammatory cytokine that is crucial in bridging innate and adaptive
185 immunity. It has several beneficial effects in the context of cancer immunotherapy, such as
186 enhancing T cell proliferation and cytotoxicity, activating and recruiting NK cells and NKT
187 cells and stimulating interferon-gamma (IFNγ) production[22]. However, its potent anti-tumour
188 effects are concomitant with severe toxicities in clinical trials, limiting its therapeutic
189 application[17]. To mitigate potential toxicity, we compared different single-chain IL-12 (scIL12)
190 constructs. We focused on two primary configurations that have previously shown different
191 biological activities[23]: One comprising the p40 subunit followed by the p35 subunit ($scIL12^{wt}$),
192 and another with the reverse arrangement p35 followed by p40 ($scIL12^{inv}$). Additionally, we
193 examined the canonical G_4S linker using different amino acid length compositions connecting
194 these subunits. This aspect was motivated by the understanding that linker length can

195 significantly influence protein flexibility[24], potentially affecting the biological activity and
196 safety profile of the scIL12 forms. To evaluate the functional differences among the various
197 scIL12s, we assessed their capacity to activate IL-12 signalling using a commercially available
198 IL-12 reporter cell line stimulated with scIL12 purified proteins. This system allows
199 quantifying the activation of IL-12 signalling, measuring the production of SEAP following
200 IL-12 binding and the subsequent activation of STAT4 (Figure 3a). The results showed that the
201 scIL12 proteins with the p35-linker-p40 subunit configuration exhibited reduced activity
202 compared to the p40-linker-p35 arrangement. Furthermore, shortening the linker length from
203 15 to 7 amino acids in the p35-linker-p40 construct resulted in an additional decrease in
204 functional activity (Figure 3b). Notably, this difference was evident only in the p35-p40
205 orientation. Further investigation of the linker length in the inverted orientation revealed no
206 correlation between shorter linker lengths and signal downregulation. Indeed, the maximum
207 reduction in signalling was achieved using a 7-amino acid linker, suggesting that this specific
208 length optimally decreases the biological activity of the inverted IL-12 construct
209 (Supplementary Figure 3a).
210 Activation of the IL-12 signalling is mediated by initial ligation of the p40 subunit to the IL-
211 12Rβ1 and subsequent heterodimerisation with IL-12Rβ2 mediated by the p35 subunit[25,26]. To
212 investigate the impact of linker length and subunit order on the structural integrity and receptor
213 binding affinity of our engineered scIL12 variants, we conducted an ELISA-based binding
214 assay. Our results revealed that the orientation of the IL-12 subunits significantly influenced
215 receptor binding. Specifically, scIL12 constructs with the p35-p40 orientation demonstrated
216 reduced binding affinity to IL-12Rβ1 compared to those with the p40-p35 orientation (Figure
217 3c). Interestingly, we observed no significant differences in binding affinity to IL-12Rβ2 across
218 the various scIL12 orientations (Supplementary Figure 3b). This indicates that the order and
219 spatial arrangement of the subunits play a crucial role in maintaining the proper conformation

220 for receptor interaction. To further evaluate the biological activity of our engineered scIL12,
221 we tested their efficacy on T cells and NK cells. The results showed that STAT4
222 phosphorylation (pSTAT4) levels varied in a specific manner, influenced by the length of the
223 linker connecting the IL-12 subunits and their orientation (Figure 3d,e). To validate the
224 functionality of scIL12 in the context of CAR-T cells, we incorporated scIL12^{wt} (p40-15aa-
225 p35) or scIL12^{inv} (p35-7aa-p40) in the IL13Rα2 c1.1^{en} CAR vector. Engineered cells were co-
226 cultured using cell-permeable supports with primary isolated T and NK cells for 72 hours to
227 assess IL-12-mediated activation through intracellular staining of pSTAT4 and measurement
228 of IFNγ production (Figure 3f). Our results demonstrated that while the IL13Rα2 c1.1^{en} +
229 scIL12^{inv} construct maintained the capacity to activate both T and NK cells, its potency was
230 notably reduced compared to the scIL12^{wt} cells (Figure 3g,h). The enhanced safety profile was
231 particularly evident in the reduced production of IFNγ, the cytokine primarily responsible for
232 IL-12 toxicity, by NK cells following IL-12 stimulation (Supplementary Figure 3c).
233 To assess both the anti-tumour efficacy and potential toxicity of our engineered scIL12 *in vivo*,
234 we utilized an aggressive mouse melanoma model using B16.F10 cells transduced to express
235 GD2. We established tumours in syngeneic mice by injecting B16.F10-GD2 cells and allowing
236 them to engraft for 8 days. Subsequently, we administered a single intravenous dose of 2.5 ×
237 10^6 GD2, GD2-mIL12^{WT}, or GD2-mIL12^{inv} CAR-T cells (Figure 3i). Our results demonstrated
238 that while GD2 CAR-T cells alone provided limited tumour control, both IL-12-expressing
239 CAR-T cell groups showed remarkable anti-tumour efficacy, with tumours remaining nearly
240 undetectable (Figure 3j and Supplementary Figure 3d). Notably, we observed a complete
241 contrast in toxicity profiles between the two IL-12 variants. Mice receiving GD2-mIL12^{wt}
242 CAR-T cells experienced significant weight loss, while mice treated with GD2-mIL12^{inv} CAR-
243 T cells maintained stable body weight, suggesting a substantially improved safety profile of
244 IL12^{inv} (Figure 3k).

245 In conclusion, our findings demonstrate that the engineered scIL12 with inverted subunit
246 orientation (p35-p40) and shortened linker length maintains a significant level of biological
247 activity while substantially reducing the systemic toxicity commonly associated with IL-12
248 therapy.

249 **HER2 as a safety switch and CAR-T detection marker**

250 To address potential safety concerns associated with IL-12 secretion, induced enhanced
251 proliferation and prolonged persistence of our CAR-T cells, we incorporated an elimination
252 switch into our construct. This safety mechanism is designed to provide a means of controlling
253 the engineered T cells *in vivo* if required[27]. For this purpose, we selected HER2 as the protein
254 of interest due to its compatibility with an existing FDA-approved targeted therapy.
255 Trastuzumab emtansine (T-DM1), an antibody-drug conjugate targeting HER2, has
256 demonstrated high efficacy and is generally well-tolerated in clinical settings[28]. In our efforts
257 to optimise the HER2-based suicide switch module, we explored various modifications to
258 enhance its efficacy while reducing its overall length in our construct (Figure 4a). Firstly, we
259 replaced the native HER2 transmembrane domain with that of CD5, a protein known to
260 facilitate rapid receptor internalisation in T cells[29]. Our results showed that cells expressing the
261 HER2-CD5 transmembrane construct exhibited significantly increased sensitivity to T-DM1
262 compared to those expressing the original HER2 construct. We further optimized the suicide
263 switch by focusing on its extracellular region. We generated a truncated version of the HER2
264 extracellular domain, retaining only the specific region containing the docking site for T-DM1
265 ($\Delta HER2^{CD5}$). This modification was designed to minimize the size of the construct while
266 preserving its essential function as a safety switch. Our results demonstrated that this truncation
267 did not compromise the construct's sensitivity to T-DM1. Remarkably, we observed a slight
268 increase in sensitivity to the antibody-drug conjugate compared to the full-length extracellular
269 domain (Figure 4b). To further validate our findings, we extended our investigation to primary

270 T cells, comparing the efficacy of T-DM1-mediated elimination between cells expressing the
271 IL13Rα2 c1.1^{en}-ΔHER2^{CD5} CAR construct and those expressing the CAR alone. T cells
272 engineered with the IL13Rα2 c1.1^{en}-ΔHER2^{CD5} CAR construct exhibited significant
273 susceptibility to T-DM1-induced elimination, whereas those expressing only the CAR
274 remained largely unaffected (Figure 4c,d). We also observed a notable decrease in CAR
275 expression intensity, suggesting that T-DM1 preferentially affects cells with higher CAR
276 expression levels. This observation indicates that the reduction of highly expressing cells,
277 which are likely responsible for increased toxicity, occurs first (Figure 4e). These findings
278 support the translational potential of our optimized suicide switch strategy for clinical
279 applications.

280 **Generation and validation of IL13Rα2 c1.1^{en} multi-armoured CAR**

281 Our findings demonstrate that each individual armoured module functions effectively within
282 the context of the IL13Rα2 c1.1^{en} CAR construct. However, combining all modules into a
283 single transgene cassette poses a significant challenge due to size constraints. Viral delivery
284 systems are typically limited to payloads of approximately 8-9kb, and larger constructs result
285 in diminished expression efficiency that correlates with their increased size[30]. To address this
286 limitation and maximise transduction efficiency, we developed an optimised two-step viral
287 production protocol. This approach involves creating an intermediate viral producer cell line
288 pseudotyped with the vesicular stomatitis virus envelope (VSV-G). This intermediate line is
289 then used to establish a stable viral producer cell line that generates viruses incorporating the
290 RD114 envelope protein, which has been shown to have superior transduction ability in
291 primary human lymphocytes[31,32] (Supplementary Figure 4a). We then tested this protocol using
292 IL13Rα2 c1.1^{en} Arm CAR, a bicistronic γ-retroviral vector encoding IL13Rα2 c1.1^{en},
293 ΔHER2^{CD5}, dsFvTBRII/CCR and IL12^{inv} all separated by a self-cleaving 2A peptide and
294 transcribed from a single promoter (Figure 5a). Upon transduction of autologous T cells with

295 this construct, we observed remarkably efficient expression of each individual component.
296 Notably, and unexpectedly, all components were expressed at a near-perfect 1:1 ratio
297 throughout the entire construct (Figure 5b). Testing the IL13Rα2 c1.1^{en} Arm CAR and IL13Rα2
298 c1.1^{en} CAR using the GBM cell line SNB19 revealed that the armoured CAR demonstrated
299 superior cytotoxic activity compared to the single CAR alone (Figure 5c). Notably, we detected
300 significantly higher levels of IFNγ production in the IL13Rα2 c1.1^{en} Arm cells, suggesting that
301 the IL12^{inv} component remained functional (Supplementary Figure 4b). We confirmed this by
302 measuring NK cell pSTAT4 levels, which showed that IL-12 was indeed present and functional
303 (Supplementary Figure 4c). To evaluate the enhanced capabilities of the IL13Rα2 c1.1^{en} Arm
304 compared to the standard IL13Rα2 c1.1^{en} CAR, we conducted a comprehensive series of stress
305 tests (Figure 5d). Our initial assessment focused on the advantages conferred by the CCR
306 module under cytokine-deprived conditions. Transduced autologous T cells were cultured
307 without cytokines for 96 hours, after which we measured their killing activity against SupT1
308 IL13Rα2 target cells. The results clearly demonstrated that IL13Rα2 c1.1^{en} Arm-modified T
309 cells exhibited superior expansion, survival, and target cell elimination efficacy in this nutrient-
310 deprived environment compared to their standard CAR counterparts (Figure 5e). We then
311 examined the cells' killing capacity following antigen stimulation in the presence of TGF-β by
312 culturing CAR-T cells on plates coated with IL13Rα2 protein and TGF-β for 96 hours before
313 assessing their cytotoxic activity. The IL13Rα2 c1.1^{en} Arm consistently outperformed the
314 IL13Rα2 c1.1^{en} CAR under these conditions (Figure 5f). To test the regulatory capability of the
315 HER2 module, we cultured the cells in the presence or absence of T-DM1. Following T-DM1
316 exposure, the cells lost their ability to kill target cells and secrete IFNγ, demonstrating effective
317 regulation through the safety switch (Figure 5g and Supplementary Figure 5d). To further
318 assess the superior performance of the IL13Rα2 c1.1^{en} Arm CAR, we conducted a stress test
319 using SNB19 glioblastoma cells. CAR-T cells were co-cultured with SNB19 cells for 7 days,

320 then transferred to freshly plated SNB19 cells for an additional 7 days. Following this extended
321 challenge, CAR-T cells were normalized and co-cultured with SUPT1-IL13Rα2 cells to
322 measure their killing activity (Figure 5h). The results demonstrated that the IL13Rα2 c1.1^{en}
323 Arm significantly outperformed the IL13Rα2 c1.1^{en} CAR, even after prolonged exposure to
324 tumour cells (Figure 5i,j). These comprehensive tests highlight the advantages of our armoured
325 CAR design, demonstrating improved persistence, killing efficiency, and maintained
326 functionality under various challenging conditions that mimic the hostile tumour
327 microenvironment. To further evaluate the IL13Rα2 c1.1^{en} Arm CAR-T cells in a more
328 physiologically relevant manner, we used a well characterised GBM tumour model by
329 orthotopically injecting U87 cells, modified to stably overexpress IL13Rα2, in
330 immunocompetent mice[33]. U87 cells were also modified to stably over-express IL13Rα2.
331 Following 8 days of engraftment, mice were grouped based on similar bioluminescence signals
332 and intracranially injected with $6.25*10^4$ CAR-T cells (Figure 5k). Remarkably while IL13Rα2
333 c1.1^{en} CAR-T cells failed to eradicate tumours in 3 out of 5 mice, complete tumour eradication
334 was achieved in all 5 mice treated with IL13Rα2 c1.1^{en} Arm CAR-T cells (Figure 5l,m,n).
335 Importantly, the body weight of the animals remained stable throughout the study, underlining
336 the safety profile of our CAR-T construct (Supplementary Figure 4e).
337 These findings collectively highlight the superior anti-tumour efficacy of our IL13Rα2 c1.1^{en}
338 Arm CAR-T cells in a clinically relevant GBM model, while also demonstrating the potential
339 for precise control of CAR-T cell activity to enhance safety.

340 **Validation of the IL13Rα2 c1.1^{en} multi-armoured CAR for clinical purpose**

341 Given the complexity of our CAR-T construct, we aimed to evaluate the feasibility of
342 manufacturing IL13Rα2 c1.1^{en} Arm CAR-T cells within a Good Manufacturing Practice
343 (GMP) workflow. We activated sorted CD3$^+$ T cells from two healthy donors using T Cell
344 TransAct™. Forty-eight hours later, these cells were transduced with clinical-grade IL13Rα2

345 c1.1^{en} Arm viral supernatant at varying multiplicities of infection (MOI). The cells were then
346 cultured using the G-Rex cell culture platform, which utilises gas-permeable membrane
347 technology to enhance oxygen delivery and nutrient exchange[34], in the presence of IL7/IL15
348 and an optimized serum-free cell culture medium (Figure 6a). Notably, we observed a dose-
349 dependent transduction efficiency, achieving a good level of CAR expression (>20%) even at
350 the lowest MOI tested, with peak expression occurring five days post-transduction (Figure 6b).
351 According to current FDA recommendations, the maximum allowable vector copy number
352 (VCN) is five copies per transduced cell for virally transduced cell therapy products[35]. Our
353 analysis of VCN seven days post-transduction confirmed that this limit was not exceeded by
354 any of the MOIs tested, demonstrating the construct's compatibility with GMP standards and
355 regulatory guidelines (Figure 6c). The expansion and propagation of the cells were monitored
356 for up to 10 days following T cell isolation. Results showed a significant increase in cell
357 numbers, with up to 30-fold expansion and an average total T cell count reaching 10^9 cells
358 (Figure 6d). Further analysis of T cell subsets revealed a shift in the composition over time.
359 There was a progressive decrease in T memory stem (Tscm) cells, accompanied by an increase
360 in effector memory T cells (Tem cells). Interestingly, the percentage of central memory (Tcm)
361 cells, a population with self-renewal capability, better persistence and antitumor immunity[36],
362 remained stable throughout the expansion period (Figure 6e). On the final day of manufacturing
363 (day 10), the CD4/CD8 ratio was approximately 1:4 (Figure 6f). The cells exhibited expression
364 of Lag3 and Tim3, with low expression of PD1 (Figure 6g). To validate the functionality of our
365 CAR-T cells at the end of the manufacturing process, we assessed their ability to kill target
366 cells. The data demonstrated that the cells maintained significant killing activity even after the
367 10-day manufacturing period (Figure 6h). Together, these data demonstrate that IL13Rα2 c1.1^{en}
368 Arm CAR-T cells can be manufactured using a GMP adaptable process while retaining their

369 cytotoxic capabilities, suggesting their potential effectiveness in targeting cancer cells upon
370 administration.

371 **DISCUSSION**

372 Recent clinical studies have demonstrated promising results for CAR-T cell therapy in GBM
373 patients. However, the efficacy of this approach has been constrained by limited CAR-T cell
374 persistence and the immunosuppressive nature of the TME. To address these challenges, we
375 describe here a novel, multi-functional CAR-T construct within a single cassette.

376 IL13Rα2 represents an exciting molecular target for cell therapy, primarily due to its specific
377 expression in GBM and its presence in cancer stem cells. Most current efforts, including
378 clinical trials, have utilised the IL13 binder known as Zetakine to target IL13Rα2. However, a
379 significant challenge with using IL-13 Zetakine is its lack of selectivity, as it also binds to
380 IL13Rα1. To address this cross-reactivity, researchers have developed a mutated form (E13Y)
381 for CAR-T cell preparation, although this approach has shown limited efficacy. Subsequent
382 enhancements included the incorporation of different co-stimulatory molecules that increased
383 efficacy[37,38,39,40]. These findings have undoubtedly contributed to the advancement of IL13Rα2
384 cell therapies for GBM. Our studies corroborated these conclusions while also revealing a
385 novel high-throughput approach to identify new binders for IL13Rα2-targeted therapy.
386 Through a humanization process, we successfully identified a new enhanced IL13Rα2 binder
387 that demonstrates high specificity for IL13Rα2. The approach enabled the generation of a
388 highly tractable single-domain antibody with enhanced selectivity for IL13Rα2, reduced
389 immunogenicity, and excellent biophysical properties, making it more suitable for development
390 as a CAR targeting domain for the treatment of GBM.

391 Two recent clinical studies involving patients with recurrent glioblastoma treated with locally
392 infused CAR-T cells demonstrated tumour reductions in nearly all participants, with substantial

393 regressions observed within 24-48 hours post-infusion. However, the majority of these
394 responses proved to be transient, with tumour recurrence noted in subsequent follow-ups[41,10].
395 One proposed solution to this challenge is the administration of repeated doses of CAR-T cells.
396 While this approach has been shown to be safe in a cohort of 65 patients, it presents significant
397 limitations in terms of feasibility, primarily due to the complexities and costs associated with
398 cell manufacturing[11]. To address these limitations, we opted for an alternative strategy focused
399 on enhancing the CAR-T cells' ability to secrete or express factors that can counteract the
400 immunosuppressive nature of the tumour microenvironment. Indeed, we focused our attention
401 on two key factors: TGF-β and IL-12.

402 TGF-β is known to induce Treg-like cell conversion and PD-1-dependent T cell exhaustion,
403 significantly inhibiting the proliferation and activity of CAR-T cells both *in vitro* and *in*
404 *vivo*[42,43,14]. To counteract this effect, we developed a novel disulfide-stabilized Fv antibody
405 targeting TGF-β receptor II, capable of blocking the downstream activation of TGF-β
406 signalling. We further innovated by coupling this antibody with the α and β chains of the GM-
407 CSF receptor to generate a constitutive active intracellular signal, leveraging the disulfide bond
408 for this purpose. The expression of this combined module led to remarkable results, with cells
409 persisting *in vitro* for over a month. These engineered cells demonstrated the ability to undergo
410 multiple rounds of expansion while maintaining impressive *in vitro* cytotoxicity even after
411 TGF-β treatment. Notably, our experiments revealed that the β/α orientation of the GM-CSF
412 receptor chains produced a more intense signal compared to the α/β configuration, as evidenced
413 by enhanced STAT5 activation. This finding suggests that our module not only offers the
414 advantage of being cytokine or stimulus-independent compared to other approaches[44], but also
415 allows for modulation based on CAR architecture or when a more dampened STAT5
416 intracellular activation is desired. While the enhanced proliferation capacity of these cells could
417 potentially lead to concerns about lymphoproliferative syndromes, our in vitro data suggest

418 that the presence of the GM-CSF CCR alone is not sufficient to cause such complications, as
419 the cells eventually undergo natural cell death. Notably, a similar approach using a signalling
420 cytokine receptor that triggers the IL-7 signalling axis (C7R) has been recently shown to be
421 well-tolerated in young patients with CNS tumours[45,46]. This suggests a low risk for adverse
422 events if our CAR T-cell and CCR combination strategy were to be employed for GBM
423 treatment.

424 IL-12 is a crucial cytokine that plays a significant role in the regulation of immune responses
425 by mainly enhancing the cytotoxic activity of NK and T cells through increased production of
426 IFNγ[47,48]. Given its powerful antitumor function, there has been considerable interest in using
427 IL-12 as an adjuvant in cell therapy and immunotherapy[49]. However, due to its potency being
428 coupled with high toxicity, recent efforts to develop more tolerable versions of the cytokine
429 have been explored. Attempts to regulate the expression of a secretable IL-12 under an
430 inducible NFAT promoter in adoptively transferred T-cell therapy still resulted in unwanted
431 toxicities due to the systemic distribution of the cytokine or a partial leakage of the NFAT gene
432 regulation system[50]. To address this issue, many research groups have explored membrane-
433 bound or -tethered approaches, sometimes coupled with locoregional delivery of CAR-T cells,
434 to limit IL-12 distribution[51,52,53]. While these strategies have demonstrated improved safety
435 profiles, they may potentially limit the full anticancer potential of IL-12 by restricting its ability
436 to activate other cell types. To avoid these limitations, we pursued a different approach to
437 harness the benefits of IL-12 while mitigating its systemic toxicity. Indeed, we leveraged the
438 heterodimeric nature of the IL-12 protein, which is composed of p35 and p40 subunits that
439 together form the biologically active IL-12p70. We created a single-chain form that expresses
440 the p35 subunit in front of the p40 ($IL12^{inv}$), a configuration known to reduce the protein's
441 biological activity. Through experimentation with various linker lengths separating the two
442 subunits, we discovered that a 7-amino acid linker most effectively decreased the biological

443 activity of the construct. Our data suggest that this reduction is primarily due to a lower affinity
444 for the IL-12Rβ1 receptor. While a more comprehensive analysis is needed, our current
445 interpretation is that inverting the two subunits either inhibits the correct folding of the protein
446 or causes the p35 subunit to mask the p40 region responsible for receptor binding.
447 Nevertheless, given that p40 binding to the receptor is the initial and limiting step in IL-12
448 signalling[25], our inverted scIL12 exhibits significantly reduced activation potency. This novel
449 approach results in a protein that still retains all the IL-12's beneficial properties but with a
450 much lower risk of systemic toxicity. In conclusion, by fine-tuning the structure and activity of
451 IL-12, we created a safer version of this potent cytokine for use in cancer immunotherapy,
452 potentially overcoming the limitations of previous strategies while maintaining its broad
453 immunostimulatory effects.

454 CAR-T therapy is generally considered safe, but severe side effects such as cytokine release
455 syndrome (CRS) and immune effector cell-associated neurotoxicity syndrome (ICANS),
456 though rare, can still occur. To address these risks, safety switches have become a crucial
457 component in cell therapy development, offering a mechanism to control or eliminate
458 engineered cells in case of severe toxicities. While various approaches are being explored, the
459 most common strategies aim to eliminate CAR-T cells entirely. Among these approaches, the
460 inducible caspase-9 suicide gene system (iCas9), ganciclovir-activated switches, and antibody-
461 dependent cell-mediated cytotoxicity (ADCC) switches are the most frequently utilised. The
462 iCas9 method has shown promising results in clinical trials[54,55], but its clinical application is
463 limited by the lack of regulatory approval for its inducer drugs (AP1903 or AP20187) in cell
464 therapy. Ganciclovir-activated switches, derived from non-human sequences, pose potential
465 immunogenicity risks, potentially inducing both humoral and cellular immune responses
466 against CAR-T cells. Given these limitations, we focused our efforts on developing an ADCC
467 switch. We engineered a truncated version of HER2, retaining only domain IV, which binds to

468 T-DM1, a safe and commercially available drug. Additionally, to enhance the internalisation
469 efficiency of the drug, we replaced the HER2 transmembrane domain with that of CD5. Our
470 preliminary results demonstrate almost complete clearance of CAR-T cells within 48 hours *in*
471 *vitro*. This approach offers a potentially safer and more clinically applicable method for
472 controlling CAR-T cell activity, addressing some of the key challenges in current safety switch
473 technologies.

474 In conclusion, our research represents a promising advancement in CAR T-cell therapy. Despite
475 recent encouraging outcomes, CAR-T cell therapy for solid tumours remains a significant
476 challenge, primarily due to the transient nature of treatment responses observed in many
477 clinical trials. These challenges are largely attributed to factors within the hostile TME. Our
478 ability to integrate multiple functional enhancements within a single construct that can still be
479 manufactured marks a substantial step forward in the field. Moreover, our findings extend
480 beyond treating GBM, as they can serve as standalone armoured modules for various CAR-T
481 constructs targeting different solid tumours. Demonstrating the feasibility of manufacturing
482 such a complex construct opens the door to incorporating diverse combinational elements
483 within a single CAR-T construct, allowing for tailored treatment strategies based on specific
484 cancer TMEs and antigens. Indeed, our data offers hope for more effective and safer treatments
485 for patients with GBM and other difficult-to-treat cancers.

MATERIAL & METHOD

Primary cells and cell culture

Peripheral Blood Mononuclear Cells (PBMCs) were isolated from Leukocyte Reduction System (LRS) cones from consented platelet apheresis donors (NHSBT, Cambridge, UK) by density centrifugation via Ficoll-Paque PLUS (GE-Healthcare; GE17-1440-03) according to manufacturer protocol. Isolated PBMCs were cultured in complete RPMI (GIBCO, ThermoFisher Scientific, Winsford, UK) supplemented with 10% Fetal Calf Serum (FBS) (Labtech, Heathfield, UK), 2mM GlutaMAX (Gibco; 35050061), IL-7 and IL-15 at ng/mL (Miltenyi Biotec, Germany).

Natural Killer (NK) cells were generated from isolated PBMCs using the CellXVivo Human NK Cell Expansion Kit (Bio-techne, R&D System, Minneapolis, US) according to the manufacturer's instructions.

Mouse splenocytes were isolated from spleens of 6- to 8-week-old C57BL/6 mice (Charles River Laboratories).

HEK-293^{GP} and HEK-293^{RD114} (Biovec Pharma, Quebec City, Canada), Phoenix-ECO (ATCC; ATCC®CRL-3214™) SNB19 (DMSZ, ACC 325 Leibniz Institute, Germany) lines were cultured in Dulbecco's Modified Eagle Medium (DMEM) (GIBCO, ThermoFisher Scientific, Winsford, UK) supplemented with 10% Fetal Calf Serum (FBS) (Labtech, Heathfield, UK) and 2mM GlutaMAX (Gibco; 35050061). HEK-Blue™ TGF-β and HEK-Blue™ IL-12 Cells (InvivoGen, Toulouse, France) lines were cultured in complete DMEM supplemented with a selection of antibiotics according to the manufacturer's instructions. SupT1 (ATCC; ATCC®CRL-1942™) and Jurkat (Clone E6, ATCC; ATCC®TIB-152™) cells were cultured in complete RPMI 1640 (GIBCO, ThermoFisher Scientific, Winsford, UK) supplemented with 10% FBS and 2mM GlutaMAX (Gibco; 35050061).

Retroviral production and Transduction

511 For amphotropic viral production, HEK-293GP cells were transiently transfected with a VSV-
512 G envelope expression plasmid and a retroviral cDNA construct (ratio 1:4). The transfection
513 was carried out with GeneJuice (Millipore; 70967-4) according to the manufacturer's
514 guidelines (ratio DNA:GeneJuice 1:2.5). After 72 h, the cell supernatant was filtered through a
515 0.45µM filter and the viral supernatant was added to HEK-293^{RD114} cells. Transduction was
516 performed by spinoculation (1500 × *g*, 1 h at 32 °C) with the addition of 10µg/ml Polybrene
517 (INSIGHT Biotechnology). Viral supernatant from HEK-293^{RD114} cells was then collected at
518 different time points when cell confluency reached ~100%, snap frozen and stored at -80 °C
519 for subsequent titration and use. Isolated PBMCs were activated using 10ng/ml IL-7 and IL-15
520 and 1:100 T Cell TransAct™ (Miltenyi Biotec). 48 hours post activation, 1x10^6 PBMCs were
521 plated on Retronectin (Takara Clonetech; T100B) on 6 well plates (Corning; 351146) with viral
522 supernatant and spun for 1500×*g*, 1 h at 32 °C.
523 For ecotropic viral production, Phoenix-ECO cells were transiently transfected with the pCL-
524 ECO packaging vector and a retroviral cDNA construct. After 72 h, the cell supernatant was
525 filtered through a 0.45µM filter and frozen. Isolated murine splenocytes were activated using
526 50ng/ml of αCD3 (Miltenyi Biotec; 130-093-387)/ αCD28 (Miltenyi Biotec; 130-093-375)
527 and 50U/ml of mIL-2 (Miltenyi Biotec; 130-120-330). 24 hours post activation, cells were
528 plated on Retronectin (Takara Clonetech; T100B) on 6 well plates (Corning; 351146) with viral
529 supernatant and spun for 1500×*g*, 1h at 32 °C

530 **Flow Cytometry**

531 Flow cytometry was performed using a MACSQuant 10 flow cytometer (Miltenyi Biotec,
532 Germany). All labelling was conducted at room temperature (RT) for 15 minutes in subdued
533 light with antibodies diluted in PBS+2% FBS. The antibody used are: αCD3-PECy7
534 (BioLegend; 300420), αCD2-PE (BioLegend; 300208), αHA-APC (BioLegend; 901524),
535 αCD56-FITC (BioLegend; 318304), αCD8-FITC (BioLegend; 344704), αProtein L (Cell

536 Signalling, 29480L), pSTAT4-AF647 (BD Biosciences, Oxford, UK 558137) αpSMAD2/3-
537 APC (BD Biosciences, Oxford, UK 562586), αHER2-FITC (R&D System, Minneapolis, US
538 FAB9589G).
539 IL13Rα2 CAR was detected using MonoRab™ Rabbit Anti-Camelid VHH Cocktail iFluor 647
540 (GenScript, Oxford,UK A02019-200).
541 Intracellular staining was performed using BD Phosflow™ Fix Buffer I and BD Phosflow™
542 Perm Buffer III (BD Biosciences, Oxford, UK) according to the manufacturer's protocol.

543 **Cytotoxicity assay**

544 Transduced cells were co-cultured with target cells at various effector:target (E:T) ratios, with
545 target cells remaining constant at $5x10^4$. Target cells are counted via flow cytometry using
546 CountBright Absolute Counting beads (Life Technologies; C36950) and cytotoxicity was
547 calculated as a percentage by normalising to the number of target cells recovered from co-
548 cultures with non-transduced (NT) T cells.

549 **Plate bound and re-stimulation assay**

550 Normalised T cells were cultured in 24-well plates previously coated overnight with 1ug/ml
551 IL13Rα2 protein and 1ug/ml TGF-β. 96h later cells were then co-cultured with SUPT1 target
552 cells and cytotoxicity was measured after 96h.
553 CAR T cells were seeded onto SNB19 cells and maintained for 7 days. Cells were harvested
554 and counted (Countess 3 Cell Counters, ThermoFisher Scientific, Winsford, UK). Cells were
555 then transferred to freshly plated SNB19 cells for repeat stimulation. 7 days later, T cells were
556 harvested, counted and finally co-cultured with SUPT1 target cells for cytotoxicity analysis at
557 the indicated E:T ratio.

558 **Cell-Free Protein Expression**

559 Proteins were produced using a cell-free expression system, specifically the PURExpress® 2.0
560 system (GeneFrontier Corporation), according to the manufacturer's protocol. Synthesized
561 constructs were derived from gBlocks® gene fragments (Integrated DNA Technologies),
562 designed to include a T7 promoter for transcription and a polyadenylation (poly A) tail for
563 stability. Each construct encoded a His-tag for subsequent purification. After transcription and
564 translation, the reaction mixtures were subjected to Ni-NTA affinity chromatography for
565 protein purification. The eluted proteins were concentrated and buffer exchanged using Amicon
566 Ultra centrifugal filters (MilliporeSigma) before downstream analyses. Protein purity and yield
567 were assessed via SDS-PAGE and Bradford assay.

568 **Mammalian Expression**

569 A separate set of proteins was produced in a mammalian expression system using the
570 pcDNA3.1(+) vector (Thermo Fisher Scientific). Constructs were designed to encode target
571 proteins fused with an Fc tag for improved stability and purification. Transient transfections
572 were performed in CHO-S cells (Thermo Fisher Scientific) cultured in CD CHO medium
573 supplemented with 8 mM L-glutamine and 1% HT supplement (Gibco). Transfections were
574 carried out using polyethylenimine (PEI) at a DNA:PEI ratio of 1:3. Following transfection,
575 cells were incubated for 5–7 days in a shaking incubator at 37°C with 5% CO_2 and 80%
576 humidity.
577 The proteins were harvested from the culture supernatant and purified using Protein A affinity
578 chromatography (GE Healthcare) under gravity flow. Eluted proteins were neutralized
579 immediately with 1 M Tris-HCl (pH 8.0) and subjected to buffer exchange into PBS using
580 Amicon Ultra centrifugal filters. The purity of the purified proteins was assessed using SDS-
581 PAGE, and concentrations were determined using a NanoDrop spectrophotometer (Thermo
582 Fisher Scientific). Proteins were stored at −80°C until further use.
583

584 **Binder Discovery and NGS sequence analysis**

585 NGS data were obtained from the MiSeq sequencing platform as two fastq files, one for
586 forward and one for reverse reads. These files were processed with an in-house python script
587 that merges forward and reverse reads assuming an overlapping region (which is always present
588 for short proteins like VHHs) to obtain the full sequence of the VHHs. The script further counts
589 the number of times each unique sequence is observed in the raw files (i.e., the number of reads
590 per unique sequence). Sequences were in silico translated to amino acids, and their count score
591 and corresponding frequency were used to sort the observed sequences from most to least
592 frequent, under the assumption that those sequences most abundant in the post-panning library
593 should be those binding most tightly to the target. All VHH sequences observed at least 3 times
594 (to reduce random sequencing errors) were aligned using the AHo numbering scheme as
595 described in [19]. The aligned CDR1, 2, and 3, were then combined and these joint CDR
596 sequences were used to determine homology groups. Specifically, each of the top 100
597 sequences by frequency in the library was considered as query, and its homology group
598 contained all sequences with a joint-CDR chemical distance smaller than 94, as calculated from
599 the distance matrix in Supplementary Figure 1a, which corresponds to around 25% CDR
600 sequence identity (this percent varies because e.g., a mutation R to K will have a much smaller
601 chemical distance than one from R to G). The assumption is that all sequences in a homology
602 group should engage the same epitope, given their highly similar CDRs. Overlapping
603 homology groups were merged. Figure 1c reports the percent frequency of the top-ranking
604 sequence used as query on the x-axis, and the sum of the percent frequencies of all sequences
605 in the homology group on the y-axis. Value labels are the ranking of the top sequence in the
606 library, with 0 corresponding to the highest frequency sequence.

607 **In vivo studies**

608 Animal studies were performed under a UK Home Office–approved project license.

609 Crown Bioscience UK Ltd carried out C57BL/6 animal studies. In brief, $1x10^5$ B16.F10 cells,
610 modified to express GD2, were subcutaneously injected into 6–10-week-old C57BL/6 female
611 mice. Eight days post engraftment $2.5x10^6$ CAR T-cells were injected intravenously and mice
612 were monitored for body weight and tumor volume using a caliper. Mice were randomized one
613 day pre-tumor injection and one day prior to treatment.
614 $5x10^4$ U87 cells, modified to express hIL13Rα2, were inoculated intracranially into NSG mice.
615 On day 7 Tumour engraftment was measured by bioluminescent imaging utilizing the IVIS
616 spectrum system (PerkinElmer, Waltham, MA) after intra-luciferin peritoneal injection and
617 mice were randomized for CAR treatment. The following day, $6.25x10^4$ CAR T-cells were
618 injected intracranially.

619 **Statistical analysis**

620 Data analyses were performed using GraphPad Prism 10 (GraphPad Software, La Jolla, USA)
621 with paired analyses as indicated. For experiments where more than two groups are compared,
622 statistical analyses were performed using one-way ANOVA followed by two-tail Student t-
623 tests. Statistical annotations were denoted with asterisks as follows: ****$P < 0.0001$,
624 ***$P < 0.001$, **$P < 0.01$, *$P < 0.05$, and not significant (ns) $P > 0.05$.

625 **Acknowledgements:**

626 We acknowledge the contribution of many people who contributed to this work either through
627 useful discussions or the provision of reagents, including Agnieszka Andres and Dr Jun Li.

628 **Author contributions:**

629 Conception and experimental design: MM, SO, SS, SC, BM
630 Computational data generation: PS, SO, AR, MG
631 Experimental data generation: MM, ES, DP, SS, RK, YY, LS, HW
632 Analysis and interpretation of data: MM, SO, SS, SC, BM

Writing: MM, SO, SS, SC, PS

Competing interests:

Maurizio Mangolini, Saket Srivastava, Emily Souster, Yajing Yang, Rajesh Karattil, Liam Schultz, Biao Ma, Diana Pombal, Shaun Cordoba and Shimobi Onuoha are current (or former) employees of Chimeris Ltd and receive (or received) salary and shares for their work.

Maurizio Mangolini, Saket Srivastava, Emily Souster, Yajing Yang, Rajesh Karattil, Liam Schultz, Biao Ma, Shimobi Onuoha are inventors on patents filed on technologies presented in the manuscript.

The contribution to this study of Pietro Sormanni, Aubin Ramon and Matthew Greenig was conducted in a consultancy capacity and was remunerated by Chimeris UK.

Data and materials availability: Transcriptomic data and accession codes will be made available upon manuscript's acceptance.

REFERENCES

1. Wu, W., Klockow, J.L., Zhang, M., Lafortune, F., Chang, E., Jin, L., Wu, Y., and Daldrup-Link, H.E. (2021). Glioblastoma multiforme (GBM): An overview of current therapies and mechanisms of resistance. Pharmacol. Res. *171*, 105780. https://doi.org/10.1016/j.phrs.2021.105780.

2. Rodgers, L.T., Villano, J.L., Hartz, A.M.S., and Bauer, B. (2024). Glioblastoma Standard of Care: Effects on Tumor Evolution and Reverse Translation in Preclinical Models. Cancers *16*, 2638. https://doi.org/10.3390/cancers16152638.

3. Land, C.A., Musich, P.R., Haydar, D., Krenciute, G., and Xie, Q. (2020). Chimeric antigen receptor T-cell therapy in glioblastoma: charging the T cells to fight. J. Transl. Med. *18*, 428. https://doi.org/10.1186/s12967-020-02598-0.

4. Wykosky, J., Gibo, D.M., Stanton, C., and Debinski, W. (2008). Interleukin-13 receptor alpha 2, EphA2, and Fos-related antigen 1 as molecular denominators of high-grade astrocytomas and specific targets for combinatorial therapy. Clin. Cancer Res. Off. J. Am. Assoc. Cancer Res. *14*, 199–208. https://doi.org/10.1158/1078-0432.CCR-07-1990.

5. Zeng, J., Zhang, J., Yang, Y.-Z., Wang, F., Jiang, H., Chen, H.-D., Wu, H.-Y., Sai, K., and Hu, W.-M. (2020). IL13RA2 is overexpressed in malignant gliomas and related to clinical outcome of patients. Am. J. Transl. Res. *12*, 4702–4714.

6. Saikali, S., Avril, T., Collet, B., Hamlat, A., Bansard, J.-Y., Drenou, B., Guegan, Y., and Quillien, V. (2007). Expression of nine tumour antigens in a series of human glioblastoma multiforme: interest of EGFRvIII, IL-13Ralpha2, gp100 and TRP-2 for immunotherapy. J. Neurooncol. *81*, 139–148. https://doi.org/10.1007/s11060-006-9220-3.

7. Brown, C.E., Warden, C.D., Starr, R., Deng, X., Badie, B., Yuan, Y.-C., Forman, S.J., and Barish, M.E. (2013). Glioma IL13Rα2 Is Associated with Mesenchymal Signature Gene Expression and Poor Patient Prognosis. PLoS ONE *8*, e77769. https://doi.org/10.1371/journal.pone.0077769.

8. Brown, C.E., Badie, B., Barish, M.E., Weng, L., Ostberg, J.R., Chang, W.-C., Naranjo, A., Starr, R., Wagner, J., Wright, C., et al. (2015). Bioactivity and Safety of IL13Rα2-Redirected Chimeric Antigen Receptor CD8+ T Cells in Patients with Recurrent Glioblastoma. Clin. Cancer Res. *21*, 4062–4072. https://doi.org/10.1158/1078-0432.CCR-15-0428.

9. Brown, C.E., Alizadeh, D., Starr, R., Weng, L., Wagner, J.R., Naranjo, A., Ostberg, J.R., Blanchard, M.S., Kilpatrick, J., Simpson, J., et al. (2016). Regression of Glioblastoma after Chimeric Antigen Receptor T-Cell Therapy. N. Engl. J. Med. *375*, 2561–2569. https://doi.org/10.1056/NEJMoa1610497.

10. Bagley, S.J., Logun, M., Fraietta, J.A., Wang, X., Desai, A.S., Bagley, L.J., Nabavizadeh, A., Jarocha, D., Martins, R., Maloney, E., et al. (2024). Intrathecal

bivalent CAR T cells targeting EGFR and IL13Rα2 in recurrent glioblastoma: phase 1 trial interim results. Nat. Med. *30*, 1320–1329. https://doi.org/10.1038/s41591-024-02893-z.

11. Brown, C.E., Hibbard, J.C., Alizadeh, D., Blanchard, M.S., Natri, H.M., Wang, D., Ostberg, J.R., Aguilar, B., Wagner, J.R., Paul, J.A., et al. (2024). Locoregional delivery of IL-13Rα2-targeting CAR-T cells in recurrent high-grade glioma: a phase 1 trial. Nat. Med. *30*, 1001–1012. https://doi.org/10.1038/s41591-024-02875-1.

12. Yang, L., Pang, Y., and Moses, H.L. (2010). TGF-beta and immune cells: an important regulatory axis in the tumor microenvironment and progression. Trends Immunol. *31*, 220–227. https://doi.org/10.1016/j.it.2010.04.002.

13. Thomas, D.A., and Massagué, J. (2005). TGF-beta directly targets cytotoxic T cell functions during tumor evasion of immune surveillance. Cancer Cell *8*, 369–380. https://doi.org/10.1016/j.ccr.2005.10.012.

14. Kloss, C.C., Lee, J., Zhang, A., Chen, F., Melenhorst, J.J., Lacey, S.F., Maus, M.V., Fraietta, J.A., Zhao, Y., and June, C.H. (2018). Dominant-Negative TGF-β Receptor Enhances PSMA-Targeted Human CAR T Cell Proliferation And Augments Prostate Cancer Eradication. Mol. Ther. J. Am. Soc. Gene Ther. *26*, 1855–1866. https://doi.org/10.1016/j.ymthe.2018.05.003.

15. Car, B.D., Eng, V.M., Lipman, J.M., and Anderson, T.D. (1999). The Toxicology of Interleukin-12: A Review. Toxicol. Pathol. *27*, 58–63. https://doi.org/10.1177/019262339902700112.

16. Jenks, S. (1996). After Initial Setback, IL-12 Regaining Popularity. JNCI J. Natl. Cancer Inst. *88*, 576–577. https://doi.org/10.1093/jnci/88.9.576.

17. Jia, Z., Ragoonanan, D., Mahadeo, K.M., Gill, J., Gorlick, R., Shpal, E., and Li, S. (2022). IL12 immune therapy clinical trial review: Novel strategies for avoiding CRS-associated cytokines. Front. Immunol. *13*, 952231. https://doi.org/10.3389/fimmu.2022.952231.

18. Asaadi, Y., Jouneghani, F.F., Janani, S., and Rahbarizadeh, F. (2021). A comprehensive comparison between camelid nanobodies and single chain variable fragments. Biomark. Res. *9*, 87. https://doi.org/10.1186/s40364-021-00332-6.

19. Ramon, A., Ali, M., Atkinson, M., Saturnino, A., Didi, K., Visentin, C., Ricagno, S., Xu, X., Greenig, M., and Sormanni, P. (2024). Assessing antibody and nanobody nativeness for hit selection and humanization with AbNatiV. Nat. Mach. Intell. *6*, 74–91. https://doi.org/10.1038/s42256-023-00778-3.

20. Marofi, F., Motavalli, R., Safonov, V.A., Thangavelu, L., Yumashev, A.V., Alexander, M., Shomali, N., Chartrand, M.S., Pathak, Y., Jarahian, M., et al. (2021). CAR T cells in solid tumors: challenges and opportunities. Stem Cell Res. Ther. *12*, 81. https://doi.org/10.1186/s13287-020-02128-1.

722 21. Righi, M., Gannon, I., Robson, M., Srivastava, S., Kokalaki, E., Grothier, T., Nannini,
723 F., Allen, C., Bai, Y.V., Sillibourne, J., et al. (2023). Enhancing CAR T-cell Therapy
724 Using Fab-Based Constitutively Heterodimeric Cytokine Receptors. Cancer
725 Immunol. Res. *11*, 1203–1221. https://doi.org/10.1158/2326-6066.CIR-22-0640.

726 22. Tugues, S., Burkhard, S.H., Ohs, I., Vrohlings, M., Nussbaum, K., Vom Berg, J., Kulig,
727 P., and Becher, B. (2015). New insights into IL-12-mediated tumor suppression. Cell
728 Death Differ. *22*, 237–246. https://doi.org/10.1038/cdd.2014.134.

729 23. Lieschke, G.J., Rao, P.K., Gately, M.K., and Mulligan, R.C. (1997). Bioactive murine
730 and human interleukin-12 fusion proteins which retain antitumor activity in vivo.
731 Nat. Biotechnol. *15*, 35–40. https://doi.org/10.1038/nbt0197-35.

732 24. Chen, X., Zaro, J.L., and Shen, W.-C. (2013). Fusion protein linkers: property, design
733 and functionality. Adv. Drug Deliv. Rev. *65*, 1357–1369.
734 https://doi.org/10.1016/j.addr.2012.09.039.

735 25. Glassman, C.R., Mathiharan, Y.K., Jude, K.M., Su, L., Panova, O., Lupardus, P.J.,
736 Spangler, J.B., Ely, L.K., Thomas, C., Skiniotis, G., et al. (2021). Structural basis for IL-
737 12 and IL-23 receptor sharing reveals a gateway for shaping actions on T versus NK
738 cells. Cell *184*, 983-999.e24. https://doi.org/10.1016/j.cell.2021.01.018.

739 26. Bloch, Y., Felix, J., Merceron, R., Provost, M., Symakani, R.A., De Backer, R.,
740 Lambert, E., Mehdipour, A.R., and Savvides, S.N. (2024). Structures of complete
741 extracellular receptor assemblies mediated by IL-12 and IL-23. Nat. Struct. Mol.
742 Biol. *31*, 591–597. https://doi.org/10.1038/s41594-023-01190-6.

743 27. Sahillioglu, A.C., and Schumacher, T.N. (2022). Safety switches for adoptive cell
744 therapy. Curr. Opin. Immunol. *74*, 190–198.
745 https://doi.org/10.1016/j.coi.2021.07.002.

746 28. García-Alonso, S., Ocaña, A., and Pandiella, A. (2020). Trastuzumab Emtansine:
747 Mechanisms of Action and Resistance, Clinical Progress, and Beyond. Trends
748 Cancer *6*, 130–146. https://doi.org/10.1016/j.trecan.2019.12.010.

749 29. Voisinne, G., Gonzalez de Peredo, A., and Roncagalli, R. (2018). CD5, an Undercover
750 Regulator of TCR Signaling. Front. Immunol. *9*, 2900.
751 https://doi.org/10.3389/fimmu.2018.02900.

752 30. Bulcha, J.T., Wang, Y., Ma, H., Tai, P.W.L., and Gao, G. (2021). Viral vector platforms
753 within the gene therapy landscape. Signal Transduct. Target. Ther. *6*, 53.
754 https://doi.org/10.1038/s41392-021-00487-6.

755 31. Sandrin, V., Boson, B., Salmon, P., Gay, W., Nègre, D., Le Grand, R., Trono, D., and
756 Cosset, F.-L. (2002). Lentiviral vectors pseudotyped with a modified RD114 envelope
757 glycoprotein show increased stability in sera and augmented transduction of
758 primary lymphocytes and CD34+ cells derived from human and nonhuman
759 primates. Blood *100*, 823–832. https://doi.org/10.1182/blood-2001-11-0042.

32. Ghani, K., Cottin, S., De Campos-Lima, P.O., Caron, M., and Caruso, M. (2009). Characterization of an alternative packaging system derived from the cat RD114 retrovirus for gene delivery. J. Gene Med. *11*, 664–669. https://doi.org/10.1002/jgm.1351.

33. Candolfi, M., Curtin, J.F., Nichols, W.S., Muhammad, A.G., King, G.D., Pluhar, G.E., McNiel, E.A., Ohlfest, J.R., Freese, A.B., Moore, P.F., et al. (2007). Intracranial glioblastoma models in preclinical neuro-oncology: neuropathological characterization and tumor progression. J. Neurooncol. *85*, 133–148. https://doi.org/10.1007/s11060-007-9400-9.

34. Ludwig, J., and Hirschel, M. (2020). Methods and Process Optimization for Large-Scale CAR T Expansion Using the G-Rex Cell Culture Platform. In Chimeric Antigen Receptor T Cells Methods in Molecular Biology., K. Swiech, K. C. R. Malmegrim, and V. Picanço-Castro, eds. (Springer US), pp. 165–177. https://doi.org/10.1007/978-1-0716-0146-4_12.

35. Center for Biologics Evaluation and Research OTAT Town Hall: Gene Therapy Chemistry, Manufacturing, and Controls.

36. Sallusto, F., Geginat, J., and Lanzavecchia, A. (2004). Central Memory and Effector Memory T Cell Subsets: Function, Generation, and Maintenance. Annu. Rev. Immunol. *22*, 745–763. https://doi.org/10.1146/annurev.immunol.22.012703.104702.

37. Kahlon, K.S., Brown, C., Cooper, L.J.N., Raubitschek, A., Forman, S.J., and Jensen, M.C. (2004). Specific Recognition and Killing of Glioblastoma Multiforme by Interleukin 13-Zetakine Redirected Cytolytic T Cells. Cancer Res. *64*, 9160–9166. https://doi.org/10.1158/0008-5472.CAN-04-0454.

38. Krebs, S., Chow, K.K.H., Yi, Z., Rodriguez-Cruz, T., Hegde, M., Gerken, C., Ahmed, N., and Gottschalk, S. (2014). T cells redirected to interleukin-13Rα2 with interleukin-13 mutein–chimeric antigen receptors have anti-glioma activity but also recognize interleukin-13Rα1. Cytotherapy *16*, 1121–1131. https://doi.org/10.1016/j.jcyt.2014.02.012.

39. Brown, C.E., Aguilar, B., Starr, R., Yang, X., Chang, W.-C., Weng, L., Chang, B., Sarkissian, A., Brito, A., Sanchez, J.F., et al. (2018). Optimization of IL13Rα2-Targeted Chimeric Antigen Receptor T Cells for Improved Anti-tumor Efficacy against Glioblastoma. Mol. Ther. *26*, 31–44. https://doi.org/10.1016/j.ymthe.2017.10.002.

40. Krenciute, G., Krebs, S., Torres, D., Wu, M.-F., Liu, H., Dotti, G., Li, X.-N., Lesniak, M.S., Balyasnikova, I.V., and Gottschalk, S. (2016). Characterization and Functional Analysis of scFv-based Chimeric Antigen Receptors to Redirect T Cells to IL13Rα2-positive Glioma. Mol. Ther. *24*, 354–363. https://doi.org/10.1038/mt.2015.199.

41. Choi, B.D., Gerstner, E.R., Frigault, M.J., Leick, M.B., Mount, C.W., Balaj, L., Nikiforow, S., Carter, B.S., Curry, W.T., Gallagher, K., et al. (2024). Intraventricular

CARv3-TEAM-E T Cells in Recurrent Glioblastoma. N. Engl. J. Med. *390*, 1290–1298. https://doi.org/10.1056/NEJMoa2314390.

42. Turley, S.J., Cremasco, V., and Astarita, J.L. (2015). Immunological hallmarks of stromal cells in the tumour microenvironment. Nat. Rev. Immunol. *15*, 669–682. https://doi.org/10.1038/nri3902.

43. Tang, N., Cheng, C., Zhang, X., Qiao, M., Li, N., Mu, W., Wei, X.-F., Han, W., and Wang, H. (2020). TGF-β inhibition via CRISPR promotes the long-term efficacy of CAR T cells against solid tumors. JCI Insight *5*, e133977. https://doi.org/10.1172/jci.insight.133977.

44. DeRenzo, C., and Gottschalk, S. (2019). Genetic Modification Strategies to Enhance CAR T Cell Persistence for Patients With Solid Tumors. Front. Immunol. *10*, 218. https://doi.org/10.3389/fimmu.2019.00218.

45. Shum, T., Omer, B., Tashiro, H., Kruse, R.L., Wagner, D.L., Parikh, K., Yi, Z., Sauer, T., Liu, D., Parihar, R., et al. (2017). Constitutive Signaling from an Engineered IL7 Receptor Promotes Durable Tumor Elimination by Tumor-Redirected T Cells. Cancer Discov. *7*, 1238–1247. https://doi.org/10.1158/2159-8290.CD-17-0538.

46. Lin, F.Y., Stuckert, A., Tat, C., White, M., Ruggieri, L., Zhang, H., Mehta, B., Lapteva, N., Mei, Z., Major, A., et al. (2024). Phase I Trial of GD2.CART Cells Augmented With Constitutive Interleukin-7 Receptor for Treatment of High-Grade Pediatric CNS Tumors. J. Clin. Oncol. *42*, 2769–2779. https://doi.org/10.1200/JCO.23.02019.

47. Seder, R.A., Gazzinelli, R., Sher, A., and Paul, W.E. (1993). Interleukin 12 acts directly on CD4+ T cells to enhance priming for interferon gamma production and diminishes interleukin 4 inhibition of such priming. Proc. Natl. Acad. Sci. *90*, 10188–10192. https://doi.org/10.1073/pnas.90.21.10188.

48. Gazzinelli, R.T., Wysocka, M., Hayashi, S., Denkers, E.Y., Hieny, S., Caspar, P., Trinchieri, G., and Sher, A. (1994). Parasite-induced IL-12 stimulates early IFN-gamma synthesis and resistance during acute infection with Toxoplasma gondii. J. Immunol. Baltim. Md 1950 *153*, 2533–2543.

49. Lasek, W., Zagożdżon, R., and Jakobisiak, M. (2014). Interleukin 12: still a promising candidate for tumor immunotherapy? Cancer Immunol. Immunother. CII *63*, 419–435. https://doi.org/10.1007/s00262-014-1523-1.

50. Zhang, L., Morgan, R.A., Beane, J.D., Zheng, Z., Dudley, M.E., Kassim, S.H., Nahvi, A.V., Ngo, L.T., Sherry, R.M., Phan, G.Q., et al. (2015). Tumor-Infiltrating Lymphocytes Genetically Engineered with an Inducible Gene Encoding Interleukin-12 for the Immunotherapy of Metastatic Melanoma. Clin. Cancer Res. *21*, 2278–2288. https://doi.org/10.1158/1078-0432.CCR-14-2085.

51. Zhang, L., Davies, J.S., Serna, C., Yu, Z., Restifo, N.P., Rosenberg, S.A., Morgan, R.A., and Hinrichs, C.S. (2020). Enhanced efficacy and limited systemic cytokine exposure with membrane-anchored interleukin-12 T-cell therapy in murine tumor

models. J. Immunother. Cancer *8*, e000210. https://doi.org/10.1136/jitc-2019-000210.

52. Hu, J., Yang, Q., Zhang, W., Du, H., Chen, Y., Zhao, Q., Dao, L., Xia, X., Natalie Wall, F., Zhang, Z., et al. (2022). Cell membrane-anchored and tumor-targeted IL-12 (attIL12)-T cell therapy for eliminating large and heterogeneous solid tumors. J. Immunother. Cancer *10*, e003633. https://doi.org/10.1136/jitc-2021-003633.

53. Lee, E.H.J., Murad, J.P., Christian, L., Gibson, J., Yamaguchi, Y., Cullen, C., Gumber, D., Park, A.K., Young, C., Monroy, I., et al. (2023). Antigen-dependent IL-12 signaling in CAR T cells promotes regional to systemic disease targeting. Nat. Commun. *14*, 4737. https://doi.org/10.1038/s41467-023-40115-1.

54. Zhou, X., Dotti, G., Krance, R.A., Martinez, C.A., Naik, S., Kamble, R.T., Durett, A.G., Dakhova, O., Savoldo, B., Di Stasi, A., et al. (2015). Inducible caspase-9 suicide gene controls adverse effects from alloreplete T cells after haploidentical stem cell transplantation. Blood *125*, 4103–4113. https://doi.org/10.1182/blood-2015-02-628354.

55. Del Bufalo, F., De Angelis, B., Caruana, I., Del Baldo, G., De Ioris, M.A., Serra, A., Mastronuzzi, A., Cefalo, M.G., Pagliara, D., Amicucci, M., et al. (2023). GD2-CART01 for Relapsed or Refractory High-Risk Neuroblastoma. N. Engl. J. Med. *388*, 1284–1295. https://doi.org/10.1056/NEJMoa2210859.

Figure 1 : *In vitro* screening identifies lead IL13Rα2 VHH for CAR-T cells

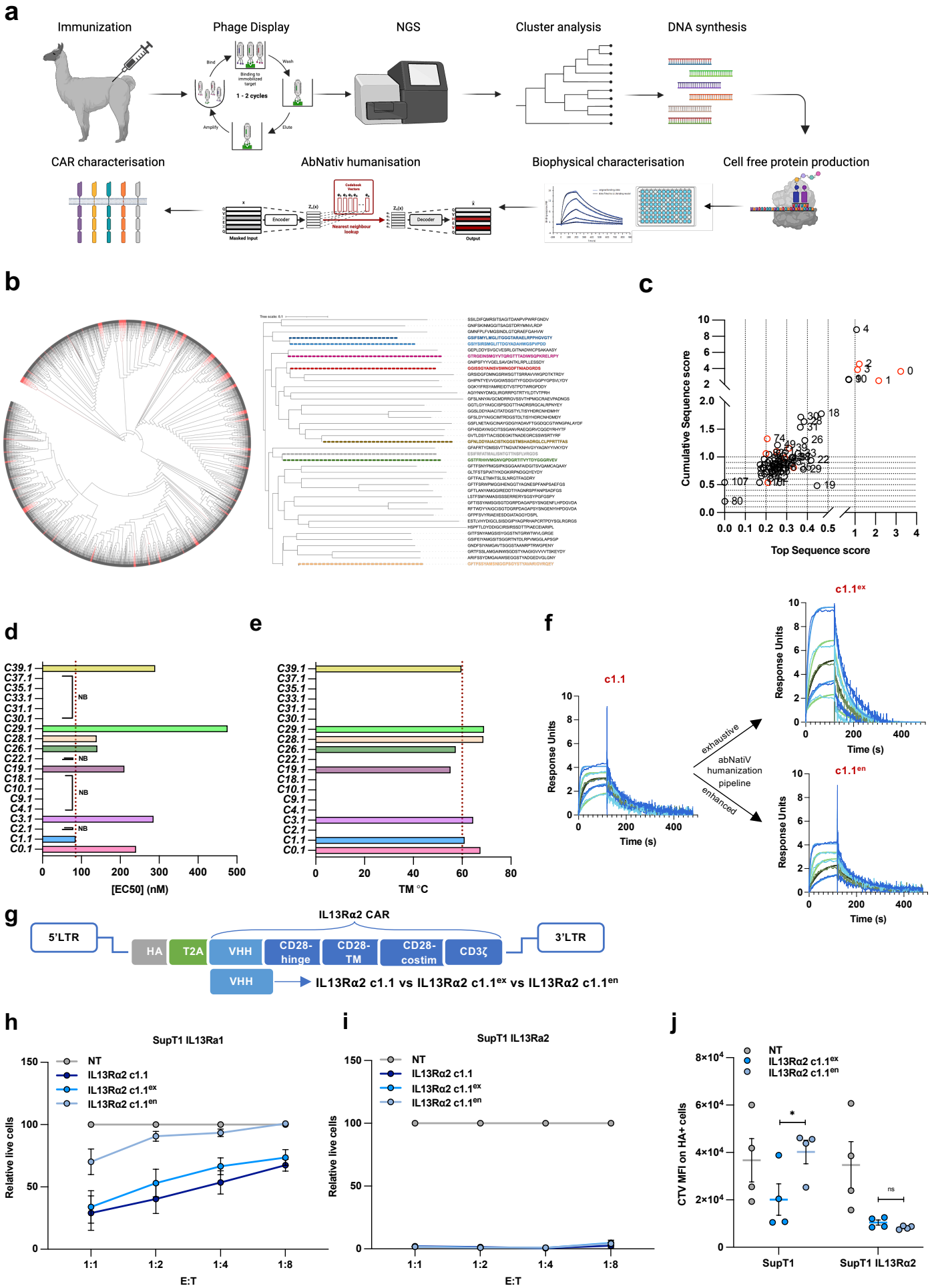

Figure 1: *In vitro* screening identifies lead IL13Rα2 VHH for CAR-T cells.

a. Graphical scheme of the experimental procedures to identify a new IL13Ra2 VHH for CAR-T cells created with BioRender.com. **b**. Phylogenetic tree generated using iTol, illustrating the complete library diversity. Clusters identified during analysis are highlighted in red. Clusters were determined by concatenating the three CDRs and analysing their diversity using a chemical space distance matrix. The sequences of the top clusters were further analysed in a unique tree to explore the distances between the combined CDRs of the highest-represented clones within the diverse clusters. **c**. Analysis of potential library bias during panning, represented as a plot of the top sequence score against the cumulative sequence score, highlighting the enrichment dynamics and selection preferences. Bar plots of the binding values (**d**) and the apparent melting temperatures (**e**) of the selected clones produced using cell-free based expression system. Values are representative measurements from three independent replicates. NB: non-binding. **f**. Binding sensorgrams of respective representative measurements showing the binding of c1.1, c.1.1^{en} and c1.1^{ex} to human IL13Rα2 by SPR. IL13Rα2 c1.1^{ex} and IL13Rα2 c1.1^{en} are based on the selected c1.1 clone and humanised using the exhaustive (^{ex}) or enhanced (^{en}) abNatiV pipeline. **g.** Schematic representation of CAR-T vectors targeting IL13Rα2. The vectors comprise an N-terminal HA-tag serving as a transduction marker, followed by the anti-IL13Rα2 VHH of interest. The VHH is linked to the transmembrane and intracellular regions of the CD28 signalling domain, which is then connected to the CD3ζ signalling domain. LTR, long terminal repeat.

SupT1 expressing IL13Rα1 (**h**) or IL13Rα2 (**i**) were co-cultured with different ratios of CAR-T cells for 72 hours. Viable target cells were quantified by flow cytometry using CD2 and CD3 expression as exclusion markers. The percentage of live target cells was calculated by normalizing to the NT group. **j**. Antigen-specific proliferation was determined by co-culturing CTV-labeled T cells with SupT1-IL13Rα2 or SupT1 cells for 96 hours. The T cells were either untransduced (NT) or expressing the IL13Rα2 c1.1^{en} or IL13Rα2 c1.1^{ex} CAR vector. *$P < 0.05$, **$P < 0.01$, ***$P < 0.001$, ****$P < 0.0001$ and not significant (ns) $P > 0.05$.

Figure 2: dsFvTBRII/CCR overcomes the inhibitory effects of TGF-β and induces CAR-T cell persistence.

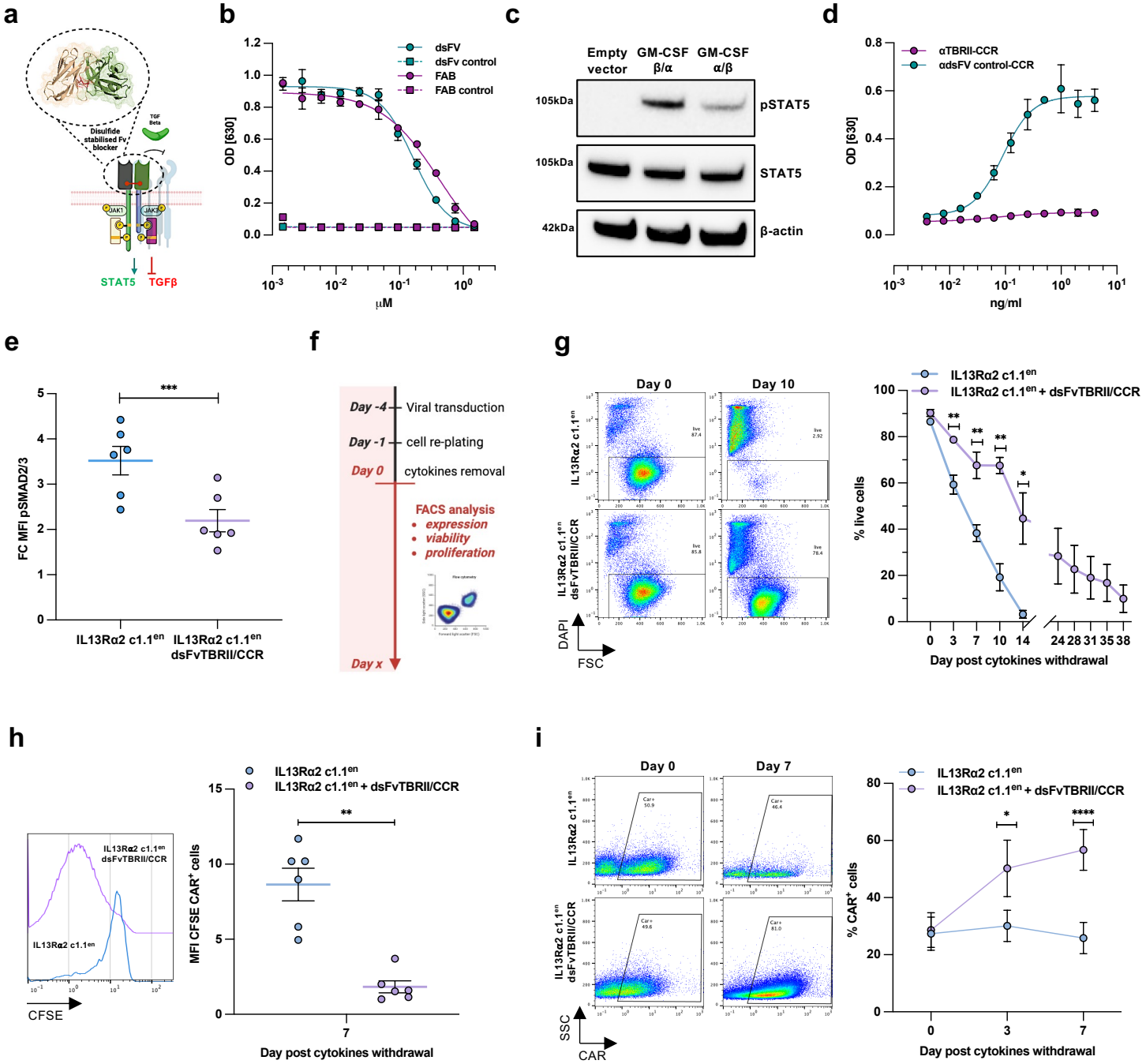

Figure 2: dsFvTBRII/CCR overcomes the inhibitory effects of TGF-β and induces CAR-T cell persistence.

a. Graphical scheme of the dsFvTBRII/CCR construct. **b.** Quantification of the SEAP secreted by HEK-Blue™ TGF-β cultured in the presence of TGF-β and the indicated level of the different TBRII blocking antibodies. **c.** Analysis of phospho-STAT5 and total STAT5 levels in Jurkat cells expressing the dsFvTBRII region fused with different orientations of the GM-CSF receptor chains: alpha-beta and beta-alpha. **d.** Quantification of the SEAP secreted by HEK-Blue™ TGF-β cultured in the presence of TGF-β and the indicated level of dsFvTBRII/CCR or a non-targeting/CCR control antibody. **e.** Quantification of intracellular phospho-SMAD2/3 levels by flow cytometry in T cells expressing IL13Ra2 c1.1^{en} CAR or IL13Ra2 c1.1^{en} CAR+dsFvTBRII/CCR exposed to 10ng/ml TGF-β for 30'. Cells were grown in serum-free media overnight before TGF-β stimulation. **f.** Schematic representation of the experimental setup. **g.** Percentage of live IL13Ra2 c1.1^{en} CAR or IL13Ra2 c1.1^{en} CAR+dsFvTBRII/CCR cells following cytokine withdrawal (n=6). Live cells were identified by DAPI exclusion by flow cytometry. **h.** Measurement of transduced T-cell proliferation by CFSE dilution 7 days post cytokine withdrawal (n=6). Cells were labelled with CFSE at day 0. **i.** Analysis of CAR-positive cell enrichment over time following cytokine withdrawal measured by flow cytometry (n=6). A representative flow cytometry plot from an individual T cell donor is presented for **g**,**h**,**i**. Cohorts are shown as mean ± SEM. Statistical analysis was done by paired t-tests. *$P < 0.05$, **$P < 0.01$, ***$P < 0.001$, ****$P < 0.0001$ and not significant (ns) $P > 0.05$. **a**,**f** were created with BioRender.com

Figure 3: scIL12^{inv} demonstrates enhanced safety while preserving its potent anti-cancer effects

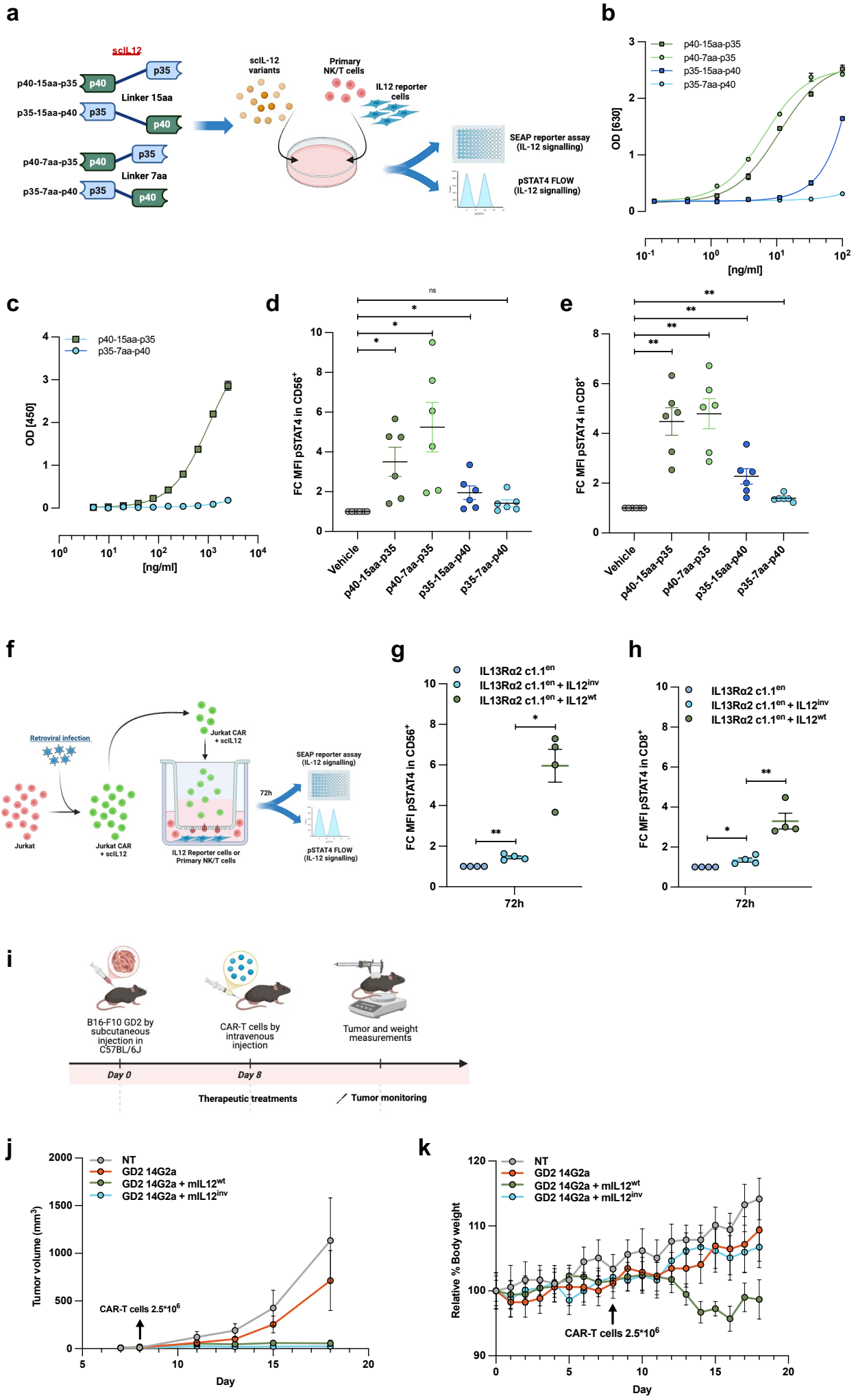

Figure 3: IL12^{inv} demonstrates enhanced safety while preserving its potent anti-cancer effects

a. Schematic representation of the protein used and the experimental layout. **b.** Quantification of the SEAP secreted by HEK-Blue™ IL12 cultured in the presence of scIL12 purified recombinant proteins at the indicated concentration for 72h. **c.** Affinity of the designed p40-15aa-p35 and p35-7aa-p40 scIL12s to the immobilized IL12β1 evaluated by ELISA assay. scIL12s were detected using an α-HIS-HRP conjugated antibody. **d,e.** CD56$^+$ and CD8$^+$ cell assay demonstrating signalling capacity of scIL-12 variants using purified recombinant protein at 100ng/ml for 30 minutes. Cells were harvested, fixed and permeabilised to detect pSTAT4 status by flow cytometry. T cells were previously activated with αCD3/CD28 in the presence of IL-2. **f.** Schematic representation of the experimental layout. **g,h.** pSTAT4 level in CD56$^+$ and CD8$^+$ cells following co-culture with Jurkat cells expressing IL13Rα2 c1.1^{en}, IL13Rα2 c1.1^{en}+IL12^{inv} or IL13Rα2 c1.1^{en}+IL12^{inv} CAR for 72h. Cells were co-cultured using a 0.4µm cell-permeable culture support. **i.** Schematic representation of the *in vivo* experimental layout created with BioRender.com. Tumor volume (**j**) and body weight (**k**) measurements of mice subcutaneously injected with $1x10^5$ GD2-expressing B16.F10 cells, which were allowed to engraft for 8 days before a $2.5x10^6$ dose of non-transduced T or CAR-T cells was intravenously injected via the tail vein. Cohorts are shown as mean ± SEM. Statistical analysis was done by paired t-tests. *$P < 0.05$, **$P < 0.01$, ***$P < 0.001$, ****$P < 0.0001$ and not significant (ns) $P > 0.05$. **a**,**i** were created with BioRender.com

Figure 4: ΔHER2^{CD5} enhances the safety of CAR T cells as safety switch

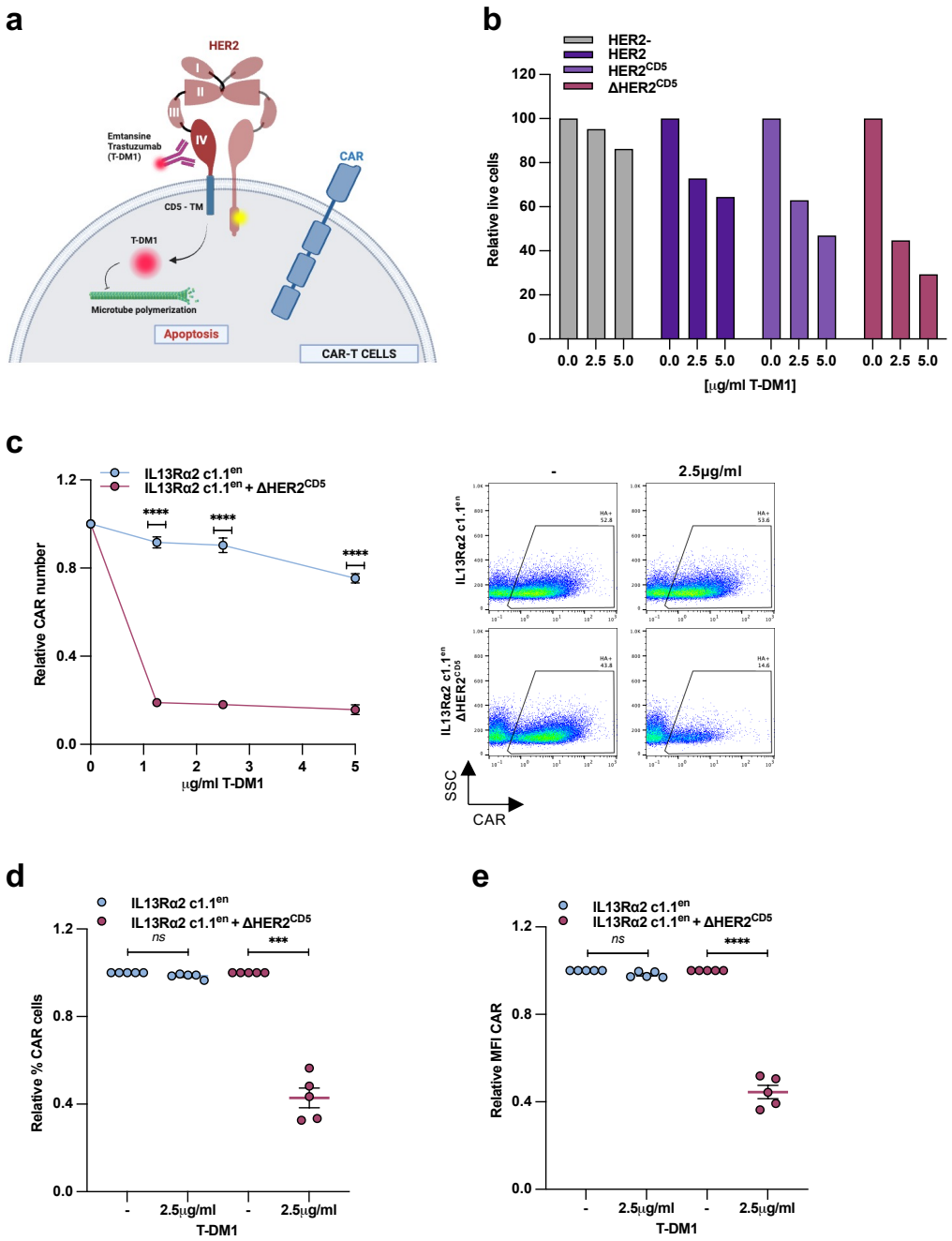

Figure 4: ΔHER2^{CD5} enhances the safety of CAR T cells as safety switch

a. Schematic representation of the HER2 mode of action as suicide switch created with BioRender.com. **b.** Relative percentage of live (DAPI^{-} Annexin-V^{-}) Jurkat cells overexpressing full length HER2, HER2 with CD5 transmembrane or truncated HER2 following T-DM1 exposure at the indicated concentrations for 48h. Results are expressed as a representative of three independent experiments. **c.** IL13Rα2 c1.1^{en} and IL13Rα2 c1.1^{en} +ΔHER2^{CD5} CAR-T cell number following 48h treatment with the indicated concentration of T-DM1 (n=6). Positive CAR-T expressing cells were counted using Precision Count Beads. A representative flow cytometry plot is shown on the right. Percentage (**d**) and MFI (**e**) of IL13Rα2 c1.1^{en} and IL13Rα2 c1.1^{en} +ΔHER2^{CD5} CAR-T cell following treatment with 2.5μg/ml of T-DM1. Cohorts are shown as mean ± SEM. Statistical analysis was done by paired t-tests. *P < 0.05, **P < 0.01, ***P < 0.001, ****P < 0.0001 and not significant (ns) P > 0.05.

Figure 5: IL13Rα2 c1.1^{en} Arm CAR shows resistance to TGF-β and enhanced cell persistence *in vitro* and *in vivo*

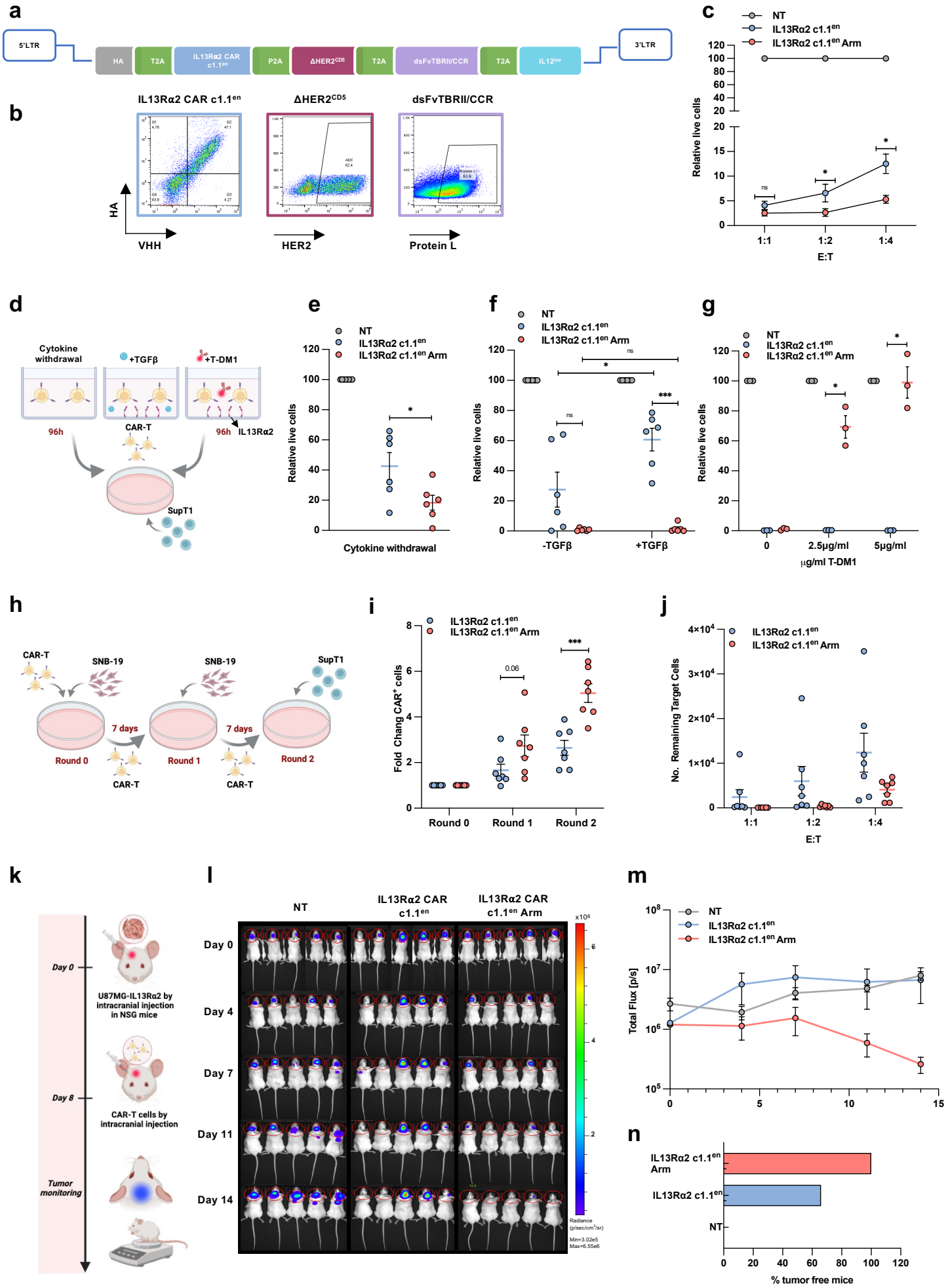

Figure 5: IL13Rα2 c1.1^{en} Arm CAR shows resistance to TGFb1 and enhanced cell persistence in vitro and in vivo

a. Schematic showing CAR vector with armouring modules. The vectors include an N-terminal transduction marker (HA) followed by the IL13Rα2 c1.1^{en}. The additional armoured modules were inserted in the indicated order and separated by self-cleaving 2a peptides. LTR, long terminal repeat. **b.** Representative flow cytometry plots showing the detection of the IL13Rα2 c1.1^{en} CAR and armoured modules. Results are expressed as representative of three independent donors for lymphocytes. **c.** Viable target SNB19 cells following co-culture with IL13Rα2 c1.1^{en} or IL13Rα2 c1.1^{en} Arm CAR-T cells at the indicated E:T ratio quantified by flow cytometry. The percentage of live target cells was calculated by normalizing to the NT group. **d.** Schematic representation of the experimental layout. In brief, CAR-T cells were cultured in a cytokine-deprived medium or in the presence of 1ug/ml IL13Rα2 immobilised protein with or without TGFβ1 or T-DM1 for 96h. A fixed volume of cells was then transferred to a plate containing SupT1-IL13Rα2 to measure their cytotoxic activity. Following another 96h, viable target cells were quantified by flow cytometry (**e**,**f**,**g**). **h.** Schematic representation of the experimental layout. In brief, CAR-T cells were co-cultured with SNB19 for 7 days (round 0) before being counted and re-seeded on fresh SNB19 for an extra 7 days (round 1). The cells were then counted, normalised and cultivated with SupT1-IL13Rα2 target cells for 48 hours (round 2). The fold increase of CAR-positive cells after each round of replating is shown in (**i**). The cytotoxic activity at the indicated E:T ratio following re-plating after round 1 is shown in (**j**). **k.** Design of the orthotopic in vivo experiment. Bioluminescence (BLI) images (**l**) and values (**m**) at day 0, 4, 7, 11 and 14 after untransduced (NT), IL13Rα2 c1.1^{en} or IL13Rα2 c1.1^{en} Arm CAR-T cells injection. **n.** Bars represent the percentage of tumor-free mice at day 14. Cohorts are shown as mean ± SEM. Statistical analysis was done by paired t-tests. *$P < 0.05$, **$P < 0.01$, ***$P < 0.001$, ****$P < 0.0001$ and not significant (ns) $P > 0.05$. **c**,**h**,**k** were created using BioRender.com

Figure 6: Validation of the IL13Rα2 c1.1^{en}multi-armoured CAR (NS007) for clinical use

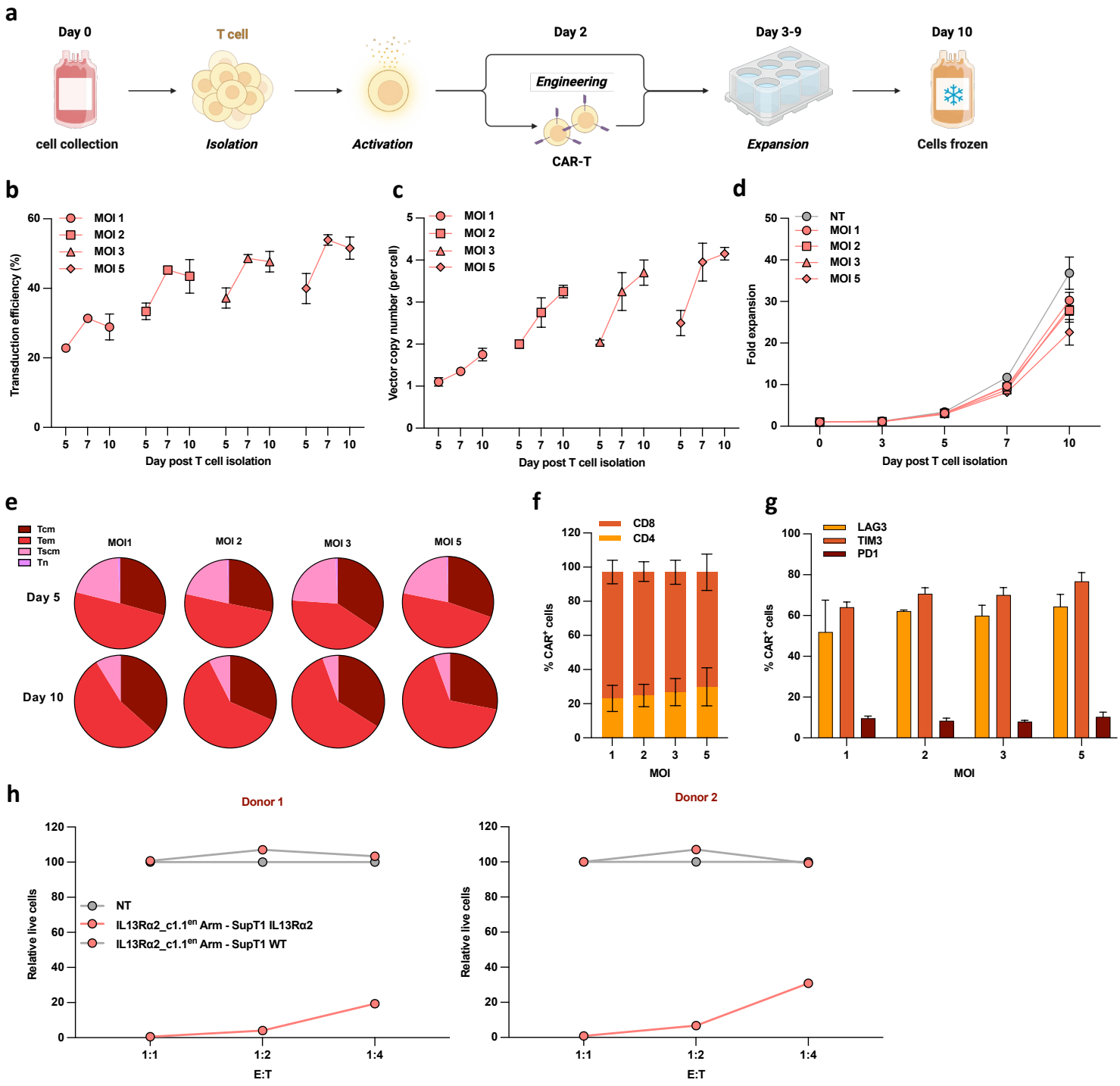

Figure 6: Validation of the IL13Rα2 c1.1^{en}multi-armoured CAR (NS007) for clinical use

a. Schematic representation of the manufacturing protocol created with biorender.com. Transduction efficiency (**b**) and vector copy number (VCN) (**c**) at day 5, 7 and 10 post T cell isolation at the indicated multiplicity of infection (MOI). **d.** Fold change in T cell expansion over a period of 10 days**. e.** Naïve (Tn), central memory (Tcm), effector memory (Tem) and memory stem cells (Tscm) T-cell subsets were identified following gating on CD45RA and CCR7 expression. Ratio of CD4:CD8 (**f**) and expression of exhaustion markers (**g**) in CAR-T positive cells 10 days post T cell isolation. **h**. Viable target SupT1-IL13Rα2 and SupT1 cells following co-culture with GMP grade manufactured IL13Rα2 c1.1en Arm CAR-T cells at the indicated E:T ratio quantified by flow cytometry. The percentage of live target cells was calculated by normalizing to the NT group. Cohorts are shown as mean ± SD of two independent healthy donors.

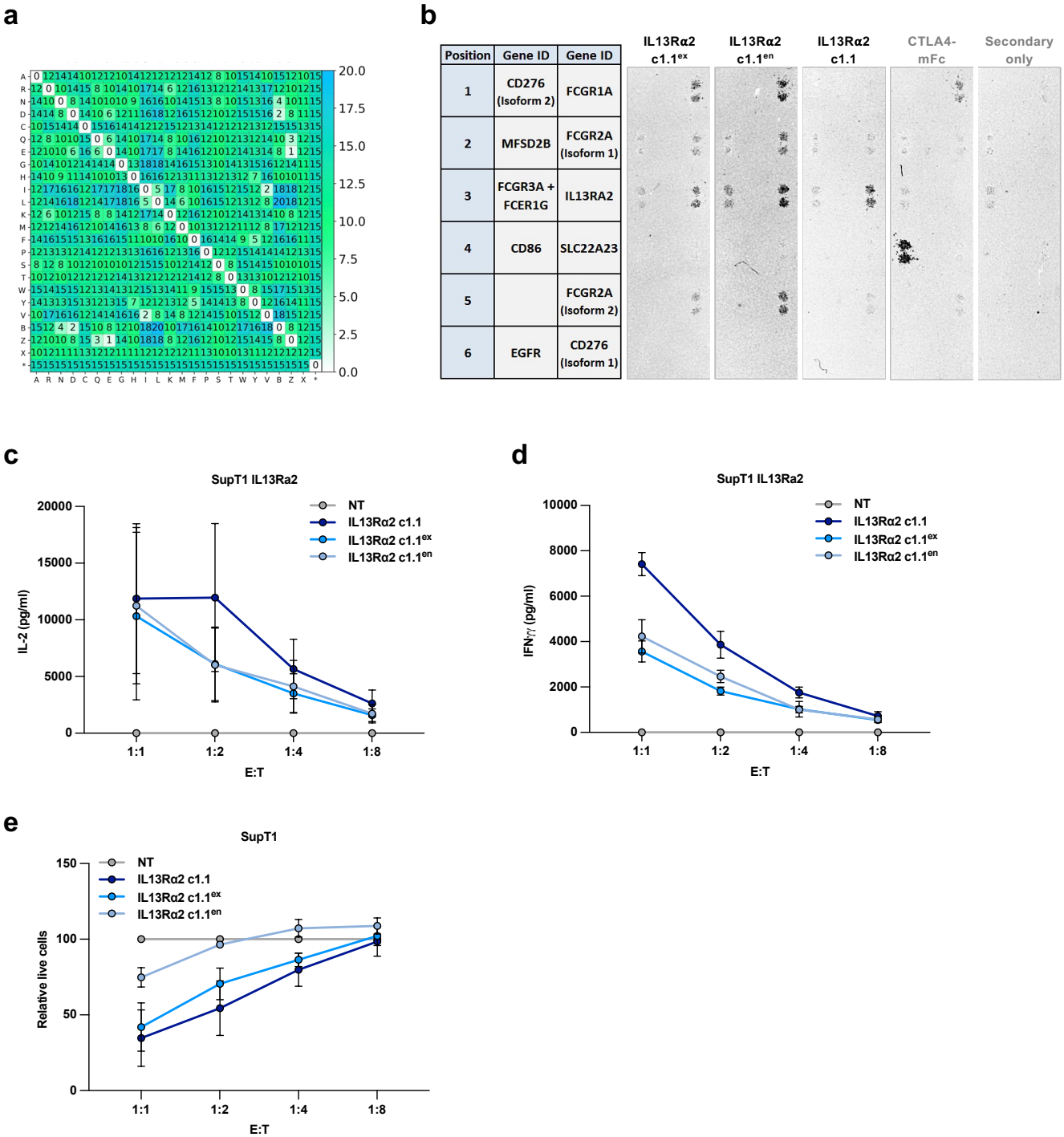

Supplementary Figure 1: *In vitro* screening identifies lead IL13Rα2 VHH for CAR-T cells.

a. Distribution matrix depicting chemical distances between amino acids based on substitution scores**. b.** The IL13Rα2 c1.1, IL13Rα2 c1.1ex, and IL13Rα2 c1.1en VHHs were Fc-conjugated and used to stain an array containing ~6000 native human membrane proteins. Binding to Fc gamma receptors (e.g., FcGR1A and FcGR2A isoforms) is expected due to the Fc conjugation. The figure shows representative intensity of the staining against selected proteins. Each column corresponds to a different VHH construct, with two dots per protein indicating duplicate spots on the array for technical validation.**c,d.** ELISA detection of IL-2 and IFN-γ production by CAR-T cells co-cultured with SupT1-IL13Rα2 cells at the indicated E:T ratio (relative to Figure 1h). **e**. Quantification of live SupT1 cells following co-culture with CAR-T cells at the indicated E:T ratio for 72h**.**

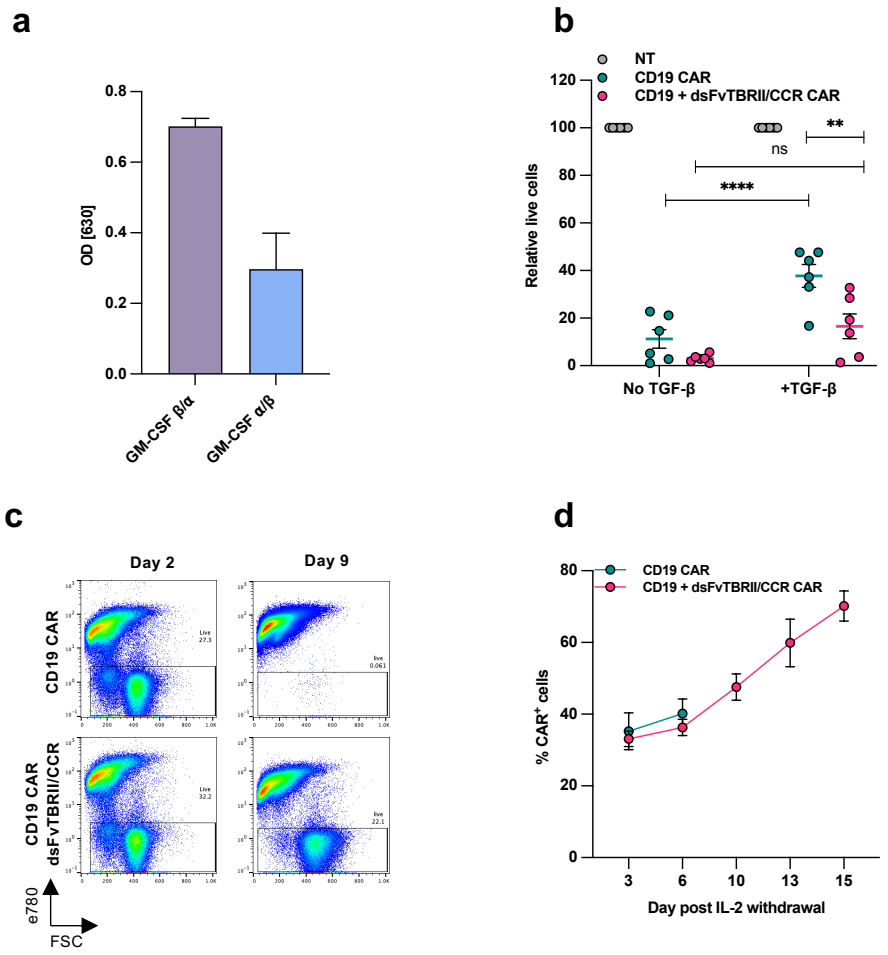

Supplementary Figure 2: dsFvTBRII/CCR overcomes the inhibitory effects of TGF-β and induces CAR-T cell persistence.

a. Quantification of the SEAP secreted by HEK-Blue™ TGF-β expressing the dsFvTBRII region fused with different orientations of the GM-CSF receptor chains: alpha-beta and beta-alpha. **b.** SupT1 expressing CD19 were co-cultured with different ratios of CAR-T cells for 72h with or without 10ng/ml TGFβ. Then, viable target cells were quantified by flow cytometry using CD2 and CD3 expression, and the percentage of live target cells was calculated by normalizing to the NT group. **c.** Representative flow cytometry plot from an individual T cell donor expressing CD19 CAR or CD19 CAR+dsFvTBRII/CCR following cytokine withdrawal at the indicated time point. A total of three independent experiments were conducted, each using lymphocytes from a different healthy donor. **d.** Analysis of CAR-positive cell enrichment over time following cytokine withdrawal measured by flow cytometry (n=3). Cohorts are shown as mean ± SEM. Statistical analysis was done by paired t-tests. *P < 0.05, **P < 0.01, ***P < 0.001, ****P < 0.0001 and not significant (ns) P > 0.05.

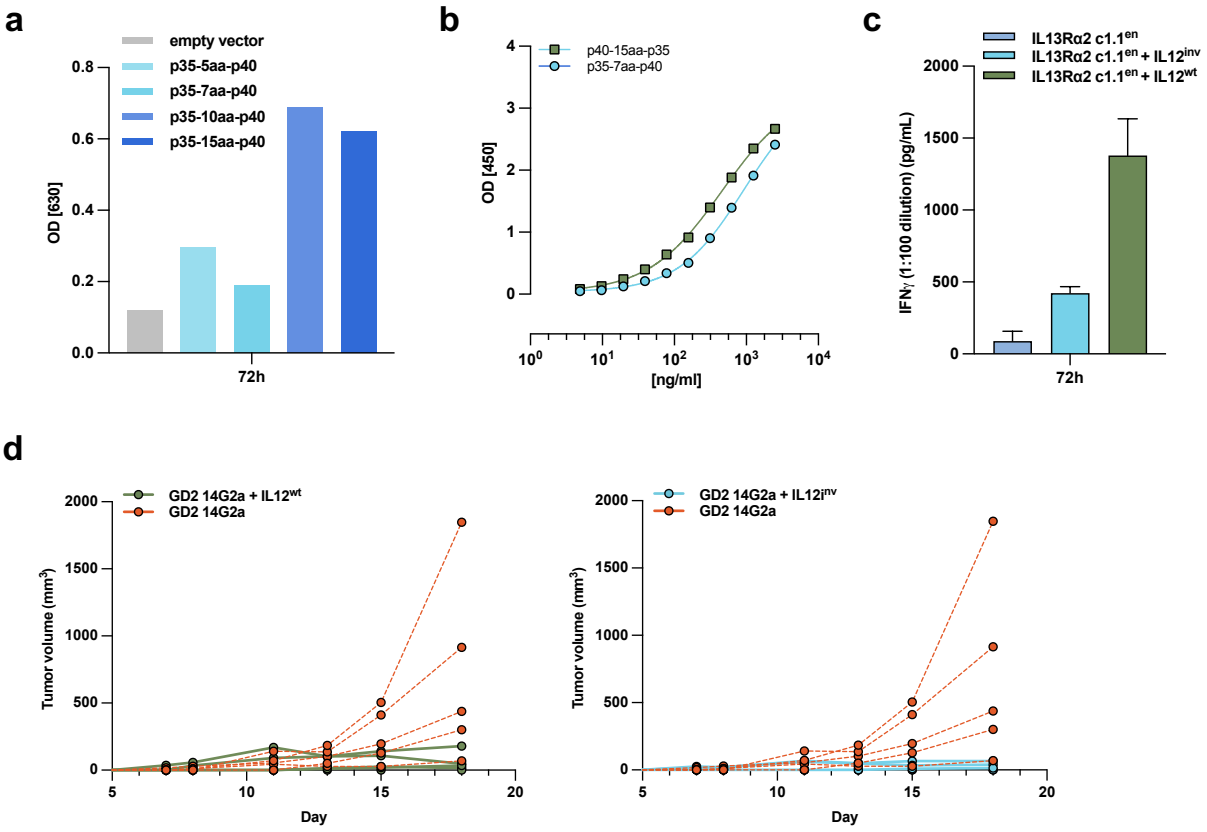

Supplementary Figure 3: scIL12^{inv} demonstrates enhanced safety while preserving its potent anti-cancer effects

a. Quantification of the SEAP secreted by HEK-Blue™ IL12 cultured in the presence of Jurkat cells expressing the p35 subunit followed by the p40 and connected with the indicated linker lengths for 72h. Results are expressed as representative of three independent experiments. **b.** Affinity of the designed p40-15aa-p35 and p35-7aa-p40 scIL12s to the immobilised IL12β2 was evaluated by ELISA assay (related to Figure 3c). **c.** ELISA detection of IFNγ production by NK cells co-cultured with Jurkat cells expressing IL13Rα2 c1.1^{en}, IL13Rα2 c1.1^{en}+IL12^{wt} or IL13Rα2 c1.1^{en}+IL12^{inv} CAR for 72h (related to Figure **3g**). Cohorts are shown as mean ± SEM **d.** Tumour volume measurement of each mouse used in the B16.F10-GD2 *in vivo* study (related to Figure **3j**).

*P < 0.05, **P < 0.01, ***P < 0.001, ****P < 0.0001 and not significant (ns) P > 0.05.

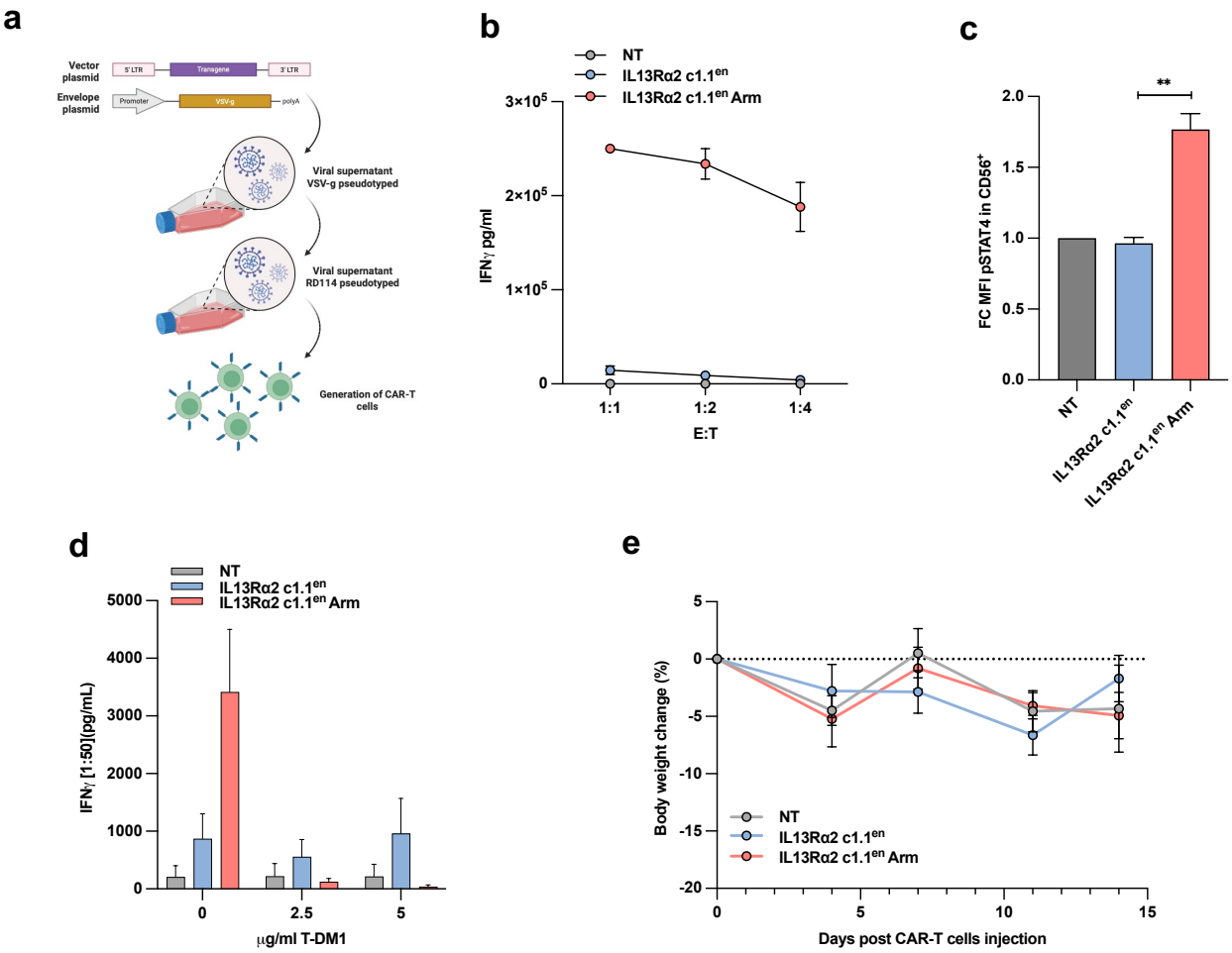

Supplementary Figure 4: IL13Rα2 c1.1^{en} Arm CAR shows resistance to TGF-β and enhanced cell persistence *in vitro* and *in vivo*

a. Schematic representation of the transduction protocol created with Biorender.com. **b.** Quantification of IFN-γ production of CAR-T cells co-cultured with SNB19 target cells (related to Figure **5c**). **c.** pSTAT4 level in CD56^{+} cells following co-culture with CAR-T cells expressing IL13Rα2 c1.1^{en} or IL13Rα2 c1.1^{en} Arm for 72h **d.** ELISA detection of IFNγ production of CAR-T cells co-cultured with SupT1-IL13Rα2 target cells following pre-exposure to T-DM1 at the indicated concentration (related to Figure **5g**). **e.** Body weight at day 0, 4, 7, 11 and 14 after untransduced (NT), IL13Rα2 c1.1^{en} or IL13Rα2 c1.1^{en} Arm CAR-T cells injection (related to Figure **5m**).